Defining the style of mineralisation at the Cairn Hill magnetite-sulphide deposit, Mount Woods Inlier, Gawler Craton, South Australia

Thesis submitted in accordance with the requirements of the University of Adelaide for an Honours Degree in Geology/Geophysics/Environmental Geoscience

Jesse Matt Clark

November 2014

THE UNIVERSITY of ADELAIDE

DEFINING THE STYLE OF MINERALISATION AT THE CAIRN HILL MAGNETITE-SULPHIDE DEPOSIT; MOUNT WOODS INLIER, GAWLER CRATON, SOUTH AUSTRALIA

HYDROTHERMAL EVOLUTION OF THE CAIRN HILL IOCG DEPOSIT

ABSTRACT

The Cairn Hill Fe-(Cu-Au) deposit is located within the World-class 1.6 Ga Olympic iron oxide-copper-gold (IOCG) Province of the Gawler Craton, South Australia. Cairn Hill deposit formation was penecontemperaneous with regional orogenesis, and is interpreted as a deep-level, 'magnetite-rich' end-member IOCG system hosted by an upper-amphibolite quartzofeldspathic ortho-gneiss and Mesoproterozoic (1600 – 1575 Ma) Hiltaba-equivalent Balta-suite granites and granodiorites. U-Pb zircon SHRIMP dating of a representative host rock and cross-cutting foliated granitic dyke, constrains the timing of mineralisation between ~1587 Ma and ~1525 Ma, respectively; suggesting an affinity to Hiltaba-age granitoids. The deposit strikes E-W over a distance of 1.3 km and is up to 40 m wide. It is characterized by two mineralised zones: the North- and South- Lodes, coincident with subsidiary structures within the transpressional Cairn Hill Shear Zone (CHSZ), and concordant with the strike of the encompassing magnetic anomaly. Progressive exhumation resulted in temperature and pressure decreases under high-fluid pressure causing the CHSZ to cross the brittle-ductile transition. This occurred relatively late in the hydrothermal-metamorphic evolution, resulting in a contractional duplex in a restraining bend suggestive of a positive flower structure providing an optimal conduit for hydrothermal fluid-flow. Early Na-Ca alteration has affected the host rocks predominantly characterised by albite + scapolite + diopside ± actinolite/titanite. Extensive K-Fe metasomatism has affected the host rocks overprinted by localised zones of intense, texturally-destructive high-temperature magnetite-biotite alteration that is typical of a transitional-style IOCG system. Associated hypogene iron mineralisation predominantly consists of magnetite, with extensive zones of a superimposed texturally-complex sulphide assemblage (pyrite-pyrrhotite-chalcopyrite). Definition of the IOCG deposit clan remains a contentious issue, primarily due to mis-classification and poor understanding of some individual deposits. Nevertheless, the general consensus is that IOCG deposits sensu-stricto represent a spectrum between high-temperature, deeper magnetite-rich end-member systems, such as Cairn Hill, and lower-temperature, shallower hematite-rich end-members.

KEYWORDS

Cairn Hill, Olympic IOCG Province, Mount Woods Inlier, Hiltaba Suite, Hydrothermal Alteration, Regional Orogenesis

TABLE OF CONTENTS

LIST OF FIGURES AND TABLES

INTRODUCTION

Definition of the Iron Oxide–Copper–Gold (IOCG) deposit clan remains a contentious issue, primarily due to mis-classification and poor understanding of many individual deposits (e.g. Skirrow *et al.* 2002; Williams *et al.* 2005; 2010; Groves *et al.* 2010; Barton 2014). Hitzman *et al.* (1992) pioneered the initial classification of iron-oxide-(Cu-U-Au-REE) deposits to incorporate a wide range of geologically-diverse deposits and considered them to represent a largely Proterozoic phenomenon. A subsequent research impasse was broken in the early 2000's (e.g. Porter volumes 2000 and 2002), which re-introduced the term iron-oxide-(copper-gold) (IOCG) systems to unify a widespread and formerly ill-defined group of deposits that share distinctive geological and chemical characteristics (e.g. Hitzman *et al.* 1992; Groves *et al.* 2010), and which also extends to younger systems (e.g. Barton 2014). Since this time controversial genetic models have led to several classification schemes based on varying characteristics (e.g. Hitzman *et al.* 1992; Williams *et al.* 2005; Groves *et al.* 2010; Barton 2014).

The 1.6 Ga Olympic Cu-Au Province is a metallogenic belt extending over 700km along the eastern margin of the Proterozoic Gawler Craton, South Australia (Skirrow *et al.* 2007; Figure 1). The Province contains a significant diversity in IOCG systems including the giant Olympic Dam Cu-Au-U deposit (Reeve et al. 1990; Haynes et al. 1995; Ehrig et al. 2013; >9000 Mt ore resource), Prominent Hill Cu-Au deposit (Belperio et al. 2004;2007; Freeman and Tomkinson 2010; >300 Mt ore resource), Carrapateena (Porter 2010), Hillside (Ismail et al. 2013), and Moonta-Wallaroo prospects(Conor et al. 2010), as well as numerous barren or weakly-mineralised systems

(Ferris et al., 2002; Direen & Lyons, 2007; Hayward and Skirrow, 2010).The variety of host rocks, alteration assemblages, mineralisation styles, and structural controls represent a spectrum characterized by two types (Bastrakov *et al.* 2007; Skirrow *et al.* 2007): paragenetically late, shallower hematite-rich end-member systems with characteristic hydrolytic (sericite) alteration (e.g. Olympic Dam, Ehrig *et al.* 2013); and paragenetically early, deeper magnetite hematite-rich systems with characteristic skarn-like calc-silicate alteration assemblages (e.g. Hillside, Ismail *et al.* 2013). The Cairn Hill Fe-(Cu-Au) deposit, the subject of this study, is within this latter group.

In this paper, we provide a comprehensive synthesis of key characteristics and parageneses of the Cairn Hill IOCG deposit. The Cairn Hill Fe-(Cu-Au) deposit is located 55km SE of Coober Pedy, South Australia and was discovered in 2005. Indicated resources as of March 2012 are 8.1Mt at 51.6% Fe, 0.37% Cu and 0.12 g/t Au (IMX Resources 2012). The hypothesis, in which Cairn Hill represents an 'end-member' deep magnetite-rich ore system, will be tested using state of the art micro-analytical techniques including reflected light microscopy and scanning electron microscopy (SEM).

Since the discovery of Prominent Hill Cu-Au deposit, the Mount Woods Inlier has received considerable attention from the mineral exploration community and is considered to remain highly prospective for undiscovered IOCG resources. However, the bulk of previous studies only targeted large (hematite-Cu-rich) systems, neglecting hundreds of smaller, magnetite-rich, distinct occurrences also with smaller alteration halos that are evident in most provinces (Barton 2014). If Cairn Hill is confirmed as a

magnetite-rich IOCG system, characterisation of the deposit and its geological setting provides major implications for regional metallogeny and crustal architecture of the Gawler Craton. In turn, this will allow development of a conceptual exploration model for the prospective Mount Woods Inlier and adjacent areas.

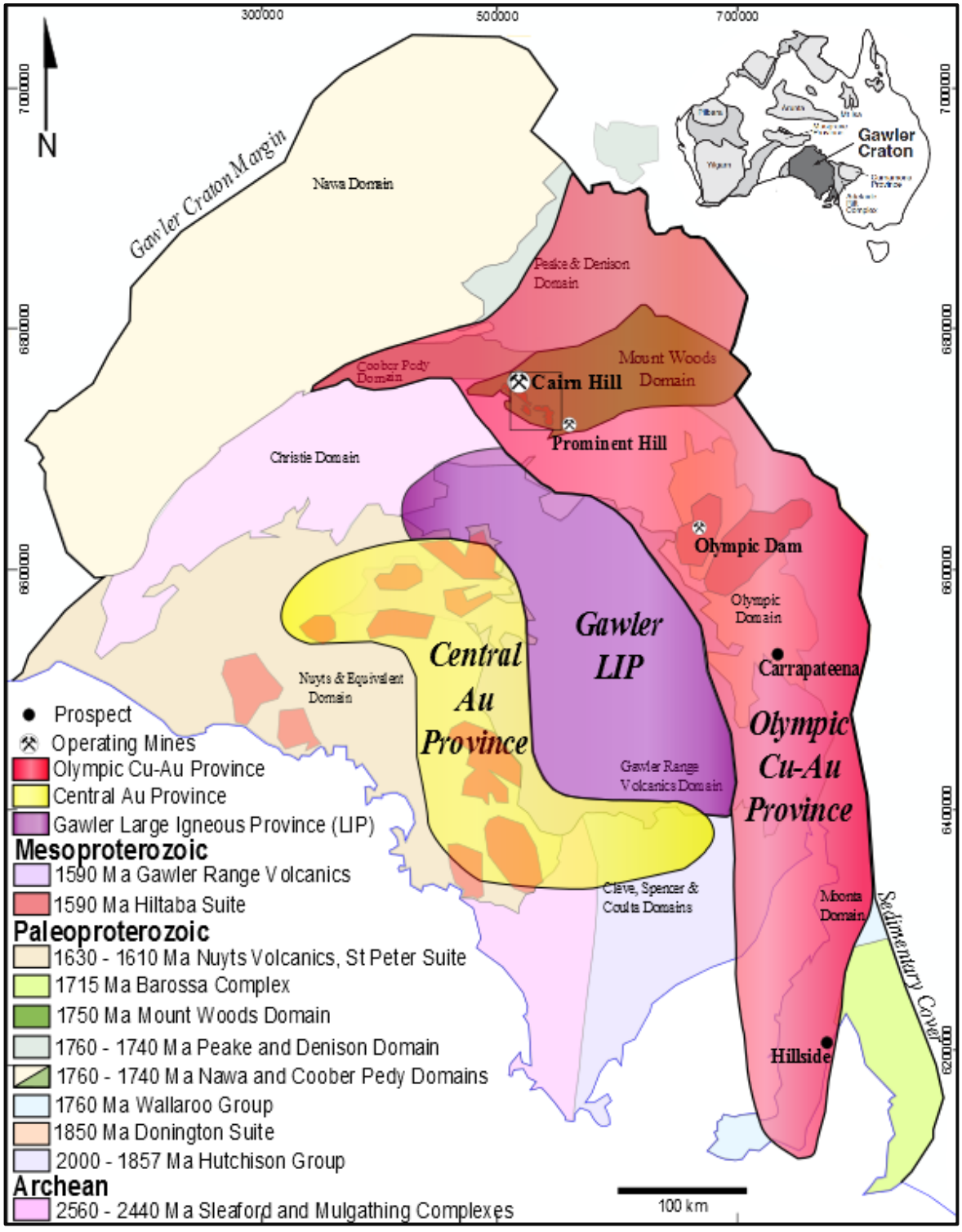

Figure 1: Location map of the Gawler Craton, South Australia illustrating the North to Northeast-trending Olympic Cu-Au (IOCG) Province, Central Au Province and the Gawler (Siliceous) Large Igneous Province (LIP). Selected, well-represented IOCG prospects and operating deposits are shown, including the Cairn Hill deposit.

REGIONAL GEOLOGICAL SETTING OF CAIRN HILL

Gawler Craton & IOCG Metallogenesis

The Gawler Craton is a stable crustal province comprised of variably deformed and metamorphosed sedimentary, volcanic and plutonic rocks spanning the late Archaean, Palaeoproterozoic and Mesoproterozoic (Hand *et al.* 2007). Due to the paucity of outcrop the geological evolution of the Craton is relatively poorly understood. Principal deformation events generating high-heat flow (up to granulite facies) include: (i) the Sleafordian Orogeny (*ca.* 2480 - 2420 Ma; Hand *et al.* 2007); (ii) Kimban Orogeny (1730 – 1690 Ma; Hand *et al.* 2007); (iii) deformation associated with emplacement of the Hiltaba Intrusive Suite (*ca.* 1595 – 1575 Ma; Daly *et al.* 1998); and, (iv) Kararan Orogeny (KO), divided into the early KO (*ca.*1690 – 1670 Ma; Teasdale *et al.* 1997) and late KO (*ca.* 1565 – 1540 Ma; Daly *et al.* 1998). These events shaped the Province before becoming tectonically stable (cratonized) at *ca.*1450 Ma (Hand *et al.* 2007).

The geological evolution of the Gawler Craton between ~1600 and ~1575 Ma includes the formation of the 1.6 Ga Olympic IOCG Province (Haywood and Skirrow, 2010), the Central Gawler Gold Province (Figure 1; Fraser and Lyons, 2006; Fraser *et al.* 2007), and a siliceous large igneous province (SLIP; Allen *et al.* 2008; Figure 1). The 'Gawler' SLIP includes oxidized (magnetite-series) A- to I- type granitoids of the 1595-1575 Ma Hiltaba Suite, and largely coeval felsic to mafic volcanic rocks of the Gawler Range Volcanics (GRV; Hand *et al.* 2007). The above suites show a temporal and sometimes spatial relationship with alteration and mineralization associated with IOCG systems.

Precambrian IOCG *sensu-stricto* deposits, including those within the Olympic Cu-Au Province, formed penecontemperaneously with supercontinental assembly and prior to break-up. Key characteristics include deposit sites located inboard of lithospheric boundaries; most commonly craton margins (D. Groves pers. Comm. 2014). Extensive mantle underplating of fertile, metasomatised sub-continent lithospheric mantle (SCLM) during prior subduction events represents a fundamental process in IOCG formation (Groves *et al.* 2010). Partial melting of buoyant metasomatised SCLM produces mafic- to ultramafic-melts enriched in volatiles and Cu and Au. Melting ponds at the Moho (crust-lithosphere) boundary and causes partial melting of the continental crust producing voluminous intermediate- to felsic-melts (Groves *et al.*2010).

Mount Woods Inlier

Cairn Hill is located within the Mount Woods Inlier (MWI) positioned at the northwestern rim of the arcuate Olympic IOCG Province. The MWI is a geologically complex region representing remnants of an accreted Palaeoproterozoic terrane comprising sparsely outcropping, poly-deformed high temperature amphibolite to granulite facies metamorphosed supracrustal rocks (e.g. Flint & Benbow 1977; Ambrose & Flint 1981; Chalmers 2007; Figure 2).

STRATIGRAPHY

The MWI comprises supracrustal rocks termed the Mount Woods Complex (Table 1). The region is blanketed by Permian to Cretaceous cover sediments (<100 m), and thickens towards the southwest away from the Inlier (Chalmers 2007a).The stratigraphy of the MWI remains a contentious issue due to poor exposure. Detailed descriptions and interpretations have evolved since Flint & Benbow (1977) and a comprehensive review

can be found in Chalmers (2007a, b) incorporating previous and current theories; a summary is given.

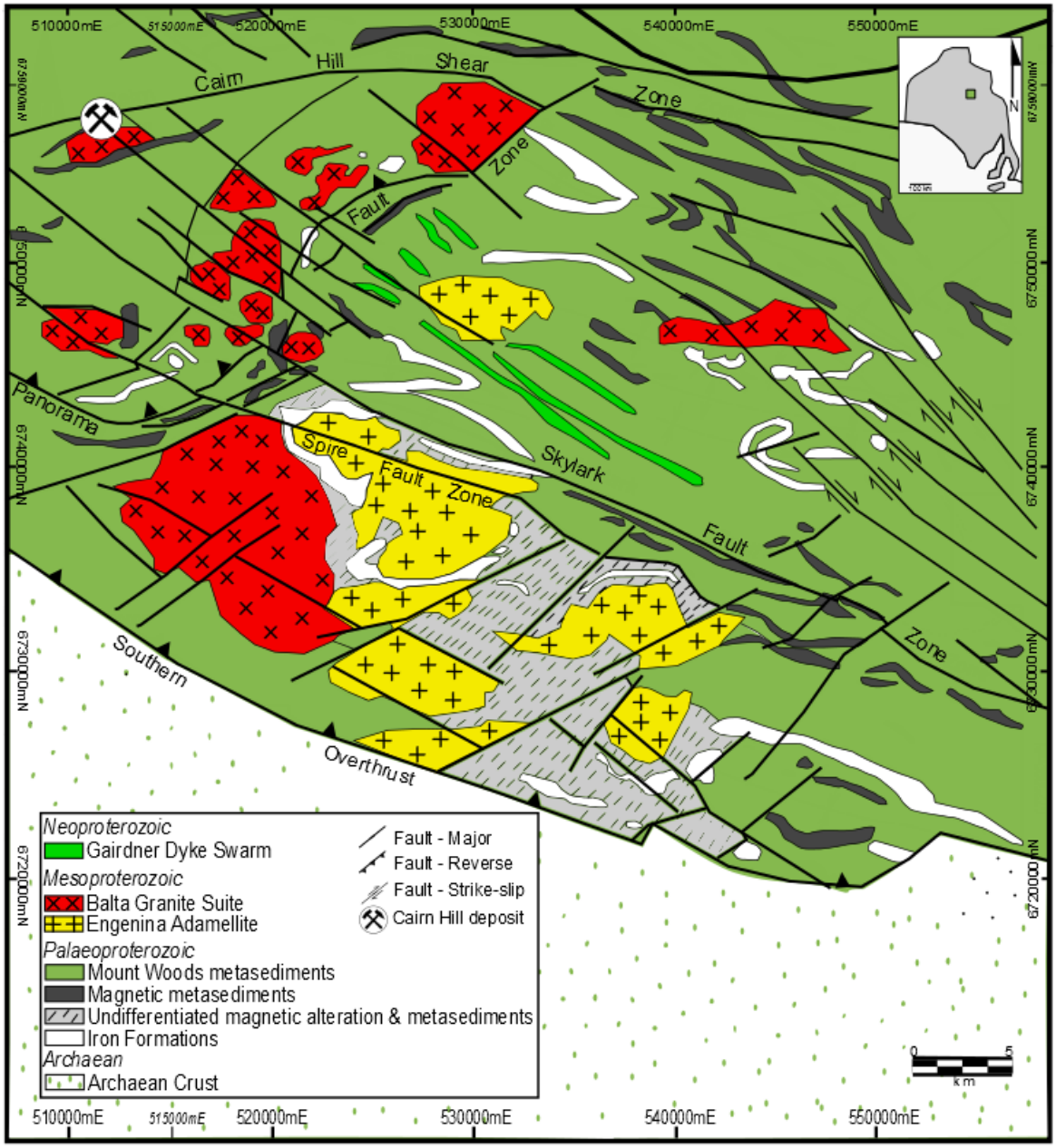

Figure 2: Interpreted geology and major structures of the Mount Woods Inlier, showing the location of the Cairn Hill deposit and Cairn Hill Shear Zone. Modified after Betts et al. (2003)

The Skylark Metasediments include multiply-deformed, amphibolite to granulite facies rocks that are commonly partially melted, and are interpreted by Chalmers (2007) to be the dominant package and represent a broad equivalent to the Wallaroo Group.

Alternatively, they may correlate with sediments from the Nawa Group- and Coober Pedy Ridge Group, and shallow to deep marine sediments of the Hutchison Group (Vassallo & Wilson 2001). Jagodzinski *et al.* (2007) determined a maximum depositional age of 1751 ± 6 Ma (U-Pb SHRIMP zircon age) for the Skylark Metasediments.

Overprinting these successions are the Palaeoproterozoic Engenina Adamellite and Mesoproterozoic bimodal intrusives, termed the Balta suite comprised of granites, granodiorites and related gabbroic bodies. These intrusives belong to the voluminous Hiltaba Suite and have a zircon U-Pb SHRIMP age of 1584± 18 Ma (Daly *et al.* 1998). A variety of I- to A-type granitic derivatives comprise the Balta Suite. These include (i) equigranular brick-red granites and clast-rich variants; (ii) coarse-grained porphyritic granite; (iii) aplitic (fine-grained)-equivalents.

Table 1: Stratigraphy of the Mount Woods Inlier. Modified after Chalmers (2007).

Super-group	Group	Formation or Equivalent
Mount Woods Complex	Balta Suite (Hiltaba Suite-equivalent)	Coarse-grained K-feldspar + plagioclase + quartz biotite magnetite granite Coarse-grained porphyritic granite Medium to fine-grained granite Coarse-grained granodiorite Gabbro Deep-red granites & clast-rich variants
	Unnamed Group	Engenina Adamellite
		Skarn/ Calc-Silicate/Dolomite Porphyroblastic Gneiss unnamed Orthogneiss unnamed Coodnambana Metaconglomerate
	Skylark Metasediments	Interbedded biotite + garnet schist & coarse quartz + feldspar gneiss Garnet + cordierite + spinel + sillimanite pelite Porphyroblastic sillimanite pelite Clast-rich (magnetic melt textured) sediment Thinly bedded psammitic + garnet pelite unit Magnetic psammite

STRUCTURE

The MWI is bound by the Karari Fault Zone in the north and the Southern Overthrust to the south. Internal shear zones greatly affect the inlier and predominantly trend E-W in the southern regions and NE-SW in the north (Betts *et al.* 2003). Due to the paucity of outcrop and subsequent lack of data the tectonothermal evolution of the MWI remains debated. Metamorphic grade ranges from greenschist to lower-amphibolite facies in the south grading to granulite facies in the north of the MWI (Forbes *et al.* 2011). Betts *et al.* (2003) provide a detailed structural analysis using geophysical techniques coupled with previous geochronology to constrain the complex evolution of the Inlier; a summary is given:

D_1 involved high-temperature (up to granulite facies) metamorphism and tight isoclinal folding (F_1) of Skylark Metasediments resulting in transposition. Timing of peak metamorphism is constrained by SHRIMP U-Pb geochronology of metamorphic monazites, yielding an age of 1736 ± 13 Ma (Fanning *et al.* 1993). Such deformation has been attributed to early stages of the Craton-wide Kimban Orogeny (*ca.* 1730-1690 Ma; Hand *et al.* 2007). D_2 resulted from ~N-S shortening, developing open to isoclinal folding (F_2) and a spaced axial planar fabric.

D_2 is interpreted to be broadly coincident with emplacement of the weakly deformed Engenina Adamellite (1692 ± 25 Ma; Flint &Benbow 1977). Discrete shear zones are interpreted to have formed in response to the early stages of the Kararan Orogeny (*ca.* 1690-1670 Ma; Betts *et al.* 2003). During this event supracrustal rocks were exhumed

and unconformably overlain by interbedded sandstones and conglomerates comprising the Coodnambana Metaconglomerate.

D_3 represents subsequent burial and high-temperature/low pressure metamorphism of unconformable Coodnambana Metaconglomerate (Forbes *et al.* 2012). Conditions of peak metamorphism are constrained to ~750ºC and ~4.5 kbar (14-16 km palaeodepth; Forbes *et al.* 2011), accompanied with metamorphic zircon U-Pb SHRIMP geochronology yielding an age of ~1590 Ma (Jagodzinski *et al.* 2007). Peak metamorphism was coincident with emplacement of the Balta Granite Suite (*ca.* 1584 ± 18 Ma; Daly *et al.* 1998). Development of a weak fabric in the Balta Granite Suite developed during the late-stages of the Kararan Orogeny (*ca.* 1565 – 1540 Ma; Betts *et al.* 2003; Hand *et al.* 2007). However, the full impact of the late-staged Kararan Orogeny in the MWI is poorly constrained.

MINERALISATION

The MWI hosts numerous barren to weakly mineralised systems that have been reported in historic exploration drill holes (Skirrow *et al.* 2002). Iron-rich metasomatic rocks are widely distributed in the MWI (Figure 2); with some zones interpreted to represent recrystallized Palaeoproterozoic BIF units (e.g. the Peculiar Knob iron-ore deposit; Freeman & Tomkinson 2010). The MWI hosts the large Prominent Hill IOCG deposit located along the Southern Overthrust defining the southern edge of the inlier. Along with the Maxman and Joes Dam Cu-Au prospects consisting of magnetite-rich alteration systems with anomalous Cu-Au-REE ± U-Co mineralisation (Hampton 1997).

APPROACH AND METHODOLOGY

Geological mapping was undertaken to understand and interpret regional and local structural and lithological diversity. Systematic petrographic-mineralogical study was carried out on weakly-altered (relatively-fresh) host rocks through to massive ore-bearing zones from representative samples located across the two operating open-pits from the Cairn Hill Mine. The sample suite covers a 1.3 km-long E-W interval, includes primary ore zones, structures and alteration assemblages and is thus considered representative.

Determination of the paragenetic diversity via identification of the primary ore mineralogy and alteration assemblages, along with accessory minerals was undertaken on 40 samples; 20 prepared as 1-inch diameter polished blocks, and the remaining 20 samples prepared as 3cm x 1cm-sized polished thin sections (Table 2). Microscopic observations were conducted using a Nikon LV100 polarizing petrographic microscope in transmitted and reflected light, and using a Quanta 450 Scanning Electron Microscope (SEM) equipped with an energy dispersive X-ray spectrometer (EDS) to provide semi-quantitative information. The SEM was operated almost exclusively in back-scatter electron mode at an accelerated voltage of 20 kv, with a spot size of ~1-2 microns.

Additionally, three diamond drill-holes, resultant of a 2013 drilling program along the strike of the deposit, were logged (approximately 1500 m; each drill-hole was drilled from surface to a depth of approximately 500 m). Core-logging was undertaken in order

to constrain; (i) paragenetic relationships; (ii) host lithologies; and, (iii) determine the depth-extent of mineralization.

Table 2: Summary of sample stratigraphy and mineralogy; refer to Figure 4 for specific sample locality.

Sample ID	Rock Type	Method	Primary Mineralogy							Minor/trace minerals	
			Kfs	Ab	Qtz	Chl	Bt	Amp	Mag	Other	REE minerals
1.1	Orebody	Pol. Block	x		**x**	x	**x**	x	**xxx**	Py,Ccp, Oam, Hem	Ap, Mnz, Thr
1.3	QFBM gneiss	Pol. Block	**xx**	**x**	x	**x**	**x**	**x**	**x**	Oam	Ap, Mnz, Thr
1.4	QFBM	Pol. Block	**xx**	**x**	x	**x**	**x**	**x**	**x**	Oam	Ap, Mnz, Thr
1.5	QFBM	Pol. Block	**xx**	**x**	x	**x**	**x**	**x**	**x**	Oam	Ap, Mnz, Thr
1.7	QFBM	Pol. Thin sec.	**xx**	**x**	x	**x**	**x**	**x**	**x**	Oam, Di, Hbl	Ap, Mnz, Thr
1.9	QFBM	Pol. Block	**xx**	**x**	x	**x**	**x**	**x**	**x**	Oam	Ap, Mnz, Thr
2.1	Granite	Pol. Thin sec.	**x**	**xx**	**x**	**x**	x	**x**	x	Oam, Di, Hbl	Xnt, Ap, Mnz
2.2	Granite	Pol. Thin sec.	**xx**	**xx**	**x**	x	x	x	x	Oam	Ap, Mnz, Thr
2.3	Granite	Pol. Thin sec.	**x**	**xx**	**x**	**x**	x	**x**	x	Oam, Di, Hbl	Ap, Mnz, Thr
2.4	Granite	Pol. Thin sec.	**xx**	**xx**	**x**	**x**	x	**x**	x	Oam	Ap, Mnz, Thr
2.7	Granite	Pol. Thin sec.	**x**	**xx**	**x**	**x**	x	**x**	x	Oam, Di, Hbl	Ap, Mnz, Thr
2.8	Orebody	Pol. Block			x	x	**x**	x	**xxx**	Py,Ccp, Oam, Hem	Ap, Mnz, Thr
2.10 (B)	Orebody	Pol. Block			x	x	**x**	x	**xxx**	Py,Ccp, Oam, Hem	Ap, Mnz, Thr
3.1	Granite	Pol. Thin sec.	**xx**	**x**	**x**	x	**x**	x	x	Oam	Ap, Mnz, Thr
3.2	Granite	Pol. Thin sec.	**xx**	**x**	**x**	x	**x**	x	x	Oam	Ap, Mnz, Thr
3.3	Orebody	Pol. Block			x	x	**x**	x	**xxx**	Oam	Ap, Mnz, Thr
3.4	QFBM	Pol. Thin sec.	x	x	x	x	x	x	**x**	Oam	Ap, Mnz, Thr
3.5	Granodiorite	Pol. Thin sec.	x	**xxx**	**xx**	x	**x**	x	x	Oam	Ap, Mnz, Thr
3.6	QFBM	Pol. Thin sec.	**xx**	**x**	x	**x**	**x**	**x**	**x**	Oam	Ap, Mnz, Thr
3.7	Orebody	Pol. Block			x	x	**x**	x	**xxx**	Py,Ccp, Oam, Hem	Ap, Mnz, Thr
4.1	Orebody	Pol. Block			x	x	**x**	x	**xxx**	Py,Ccp, Oam, Hem	Ap, Mnz, Thr
4.2	Granite	Pol. Thin sec.	**xx**	**xx**	**x**	**x**	x	**x**	x	Oam	Ap, Mnz, Thr
5.1	Mylonite	Pol. Thin sec.	**xx**	**x**	**xx**	**x**	**xx**	**x**	**x**	Oam, Di, Hbl	Ap, Mnz, Thr
5.2	MB Schist	Pol. Thin sec.			x	x	**x**	x	**xxx**	Oam	Ap, Mnz, Thr
5.3	Granite	Pol. Thin sec.	**xx**	**xx**	**x**	**x**	x	**x**	x	Oam	Ap, Mnz, Thr
5.4	Shear Zone	Pol. Block			**xxx**	**x**	**xx**	**x**	x	Oam, Di, Hbl	Ap, Mnz, Thr
5.5	MB Schist	Pol. Block			x	x	**x**	x	**xxx**	Oam	Ap, Mnz, Thr
5.6	Mylonite	Pol. Thin sec.	**xx**	**x**	**xx**	**x**	**xx**	**x**	**x**	Oam	Ap, Mnz, Thr
5.7	Mylonite	Pol. Block	**xx**	**x**	**xx**	**x**	**xx**	**x**	**x**	Oam, Di, Hbl	Ap, Mnz, Thr
5.8	Mylonite	Pol. Block	**xx**	**x**	**xx**	**x**	**xx**	**x**	**x**	Oam	Ap, Mnz, Thr
5.9	Mylonite	Pol. Thin sec.	**xx**	**x**	**xx**	**x**	**xx**	**x**	**x**	Oam, Di, Hbl	Ap, Mnz, Thr
6.1	Granite	Pol. Block	**xx**	**x**	**xx**	**x**	**xx**	**x**	**x**	Oam, Di, Hbl	Ap, Mnz, Thr
6.2	Supergene	Pol. Thin sec.			x	**xxx**		**xxx**	x	Hem, Mht, Ser, Cc, Cu^o	Mnz
6.3	Orebody	Pol. Block			x	x	**x**	x	**xxx**	Py,Ccp, Oam, Hem	Ap, Mnz, Thr
6.4	Granite	Pol. Thin sec.	**xx**	**x**	**xx**	**x**	**xx**	**x**	**x**	Oam	Ap, Mnz, Thr
6.5	Granite	Pol. Thin sec.	**xx**	**x**	**xx**	**x**	**xx**	**x**	**x**	Oam	Ap, Mnz, Thr
6.6	Granite	Pol. Thin sec.	**xx**	**x**	**xx**	**x**	**xx**	**x**	**x**	Oam	Ap, Mnz, Thr
6.7	Orebody	Pol. Block	x	x	x	x	x	x	**xxx**	Oam	Ap, Mnz, Thr
6.8	Orebody	Pol. Block	x	x	x	x	x	x	**xxx**	Py,Ccp, Oam, Hem	Ap, Mnz, Thr
6.9	MB Schist	Pol. Block			x	x	**x**	x	**xxx**	Oam	Ap, Mnz, Thr
6.10 (B)	MB Schist	Pol. Block			x	x	**x**	x	**xxx**	Oam	Ap, Mnz, Thr
PC-HEM	Supergene	Pol. Block			x	**xx**		**xx**	x	Hem, Mht, Ser, Cc, Cu^o	Mnz

*Abbreviations: K-feldspar (Kfs); albite (Ab); quartz (Qtz); chlorite (Chl); biotite (Bt); amphibole (Amp); magnetite (Mag); pyrite (Py); chalcopyrite (Ccp); orthoamphibole (Oam); diopside (Di); hornblende (Hbl); hematite (Hem); maghemite (Mht); chalcocite (Cc); native copper (Cu^o); apatite (Ap); monazite (Mnz); xenotime (Xnt); thorite (Thr); sericite (Ser); polished (Pol.); section (sec.); magnetite-biotite (MB). Compositions: **xxx** >50%; **xx** = 50-20%; **x** = 20-5%; x<5%.*

DEPOSIT GEOLOGY

Geological Setting

The Cairn Hill Fe-Cu-Au deposit is located within the hanging-wall of the long-lived, E-NE to W-SW trending transpressional Cairn Hill Shear Zone (CHSZ). The CHSZ is a wide structural corridor evidenced by multiple brittle-ductile faults and shear zones defining the northern edge of the Mount Woods Domain (Figure 2). The deposit strikes E-W over a distance of 1.3 km, is up to 40 m wide, and consists of two mineralised zones: the North- and South- Lodes. These mineralized zones are coincident with a set of parallel subsidiary faults and shear zones within the CHSZ and are concordant with the strike of the encompassing magnetic anomaly, which can extend to a strike-distance of approximately 15 km (Figure 3).

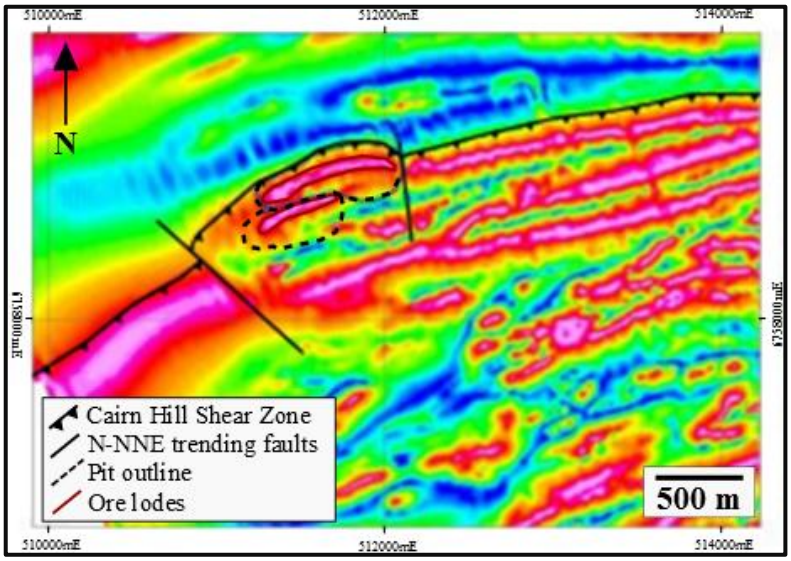

Figure 3: Magnetic response of the area surrounding the Cairn Hill deposit, with Pit 1 outlined. The long-lived, E-W striking Cairn Hill Shear Zone and later, cross-cutting N-NNE- trending structures are shows. (Modified after IMX Resources, 2012)

Mineralisation is hosted by a complex suite predominantly comprised of mid-to-upper amphibolite facies quartzofeldspathic granites and gneisses (Figure 4). Host rocks are

unconformably overlain by early-Palaeozoic to late-Tertiary aged flat-lying sedimentary rocks (Chalmers 2007a). The thickness of cover sequences varies from 0-45 m directly above the North- and South- lodes but thickens considerably towards the west of the deposit (>100 metres), thus limiting the economic viability of possible extensions along strike of the magnetic anomaly.

Lithologies

Lithological nomenclature of host rocks at the Cairn Hill deposit often proved difficult due to the broad similarity of mineral associations and colouring, along with variable intensities of deformation and strain rates in the quartz-K-feldspar-biotite-gneiss and altered alkali-rich intrusives.

MESOPROTEROZOIC BALTA SUITE INTRUSIVES

Alkali-rich (syeno-)granite

Unaltered specimens are characterized by pink-red colour, and are medium-to-coarse-grained (<1 cm), hypidiomorphic equigranular alkali-rich granite to syenogranite composition. The approximate modal composition is 50% alkali feldspar 20-25% sodic-plagioclase (albite) 20-25% quartz, 5-10% biotite and amphibole (hornblende) with accessory magnetite, titanite, apatite, and zircon. A localised foliation is defined by the alignment of metamorphic biotite and minor magnetite. The prominent foliation paired with characteristic elongate quartz ribbons that are evident is suggestive of a LS-tectonite geometry implying non-coaxial strain. The granitic host rocks also display local graphic textures.

Granodiorite dyke

Minor weakly-foliated fine-grained (<0.5 cm) granodiorite dykes occupy a unique structural position within the Northern ore-lode defined by a wide (<5 m) dyke clearly cross-cutting the mineralisation providing a lower constraint for timing. Minor dykes (< 0.5 m) cross-cut host lithologies proximal to the principal, wide dyke but are not abundant. The dykes are characterised by a grey-white colour, are hypidiomorphic and equigranular granomonzonite-to-granodiorite composition. The approximate modal composition is 50-55% sodic- and calcic- plagioclase (albite-oligoclase) 20-25% K-feldspar (orthoclase-microcline) 20-25% quartz, and minor (1-5%) biotite, magnetite and amphibole (hornblende).

Pegmatite and aplite dykes

Subordinate pegmatite dykes and aplite-horizons are evident across the deposit, cross-cutting most host-lithologies and are interpreted to represent late-to-final phases of the Balta Suite. Both lithotypes are compositionally-similar to the alkali-rich granites; however, both lack sodic (and/or calcic-) plagioclase and are instead dominated by a quartz-K-feldspar-rich assemblage with relatively abundant tourmaline (5-10%).

Gabbro

Less abundant gabbro interpreted from deeper drill-core intervals (approximately at depths >200 m) as narrow dykes forming early with respect to initial high-temperature alteration stages; unaltered specimens were not observed. The dykes are fine-grained equigranular holocrystalline intrusive rocks, with remnant primary minerals

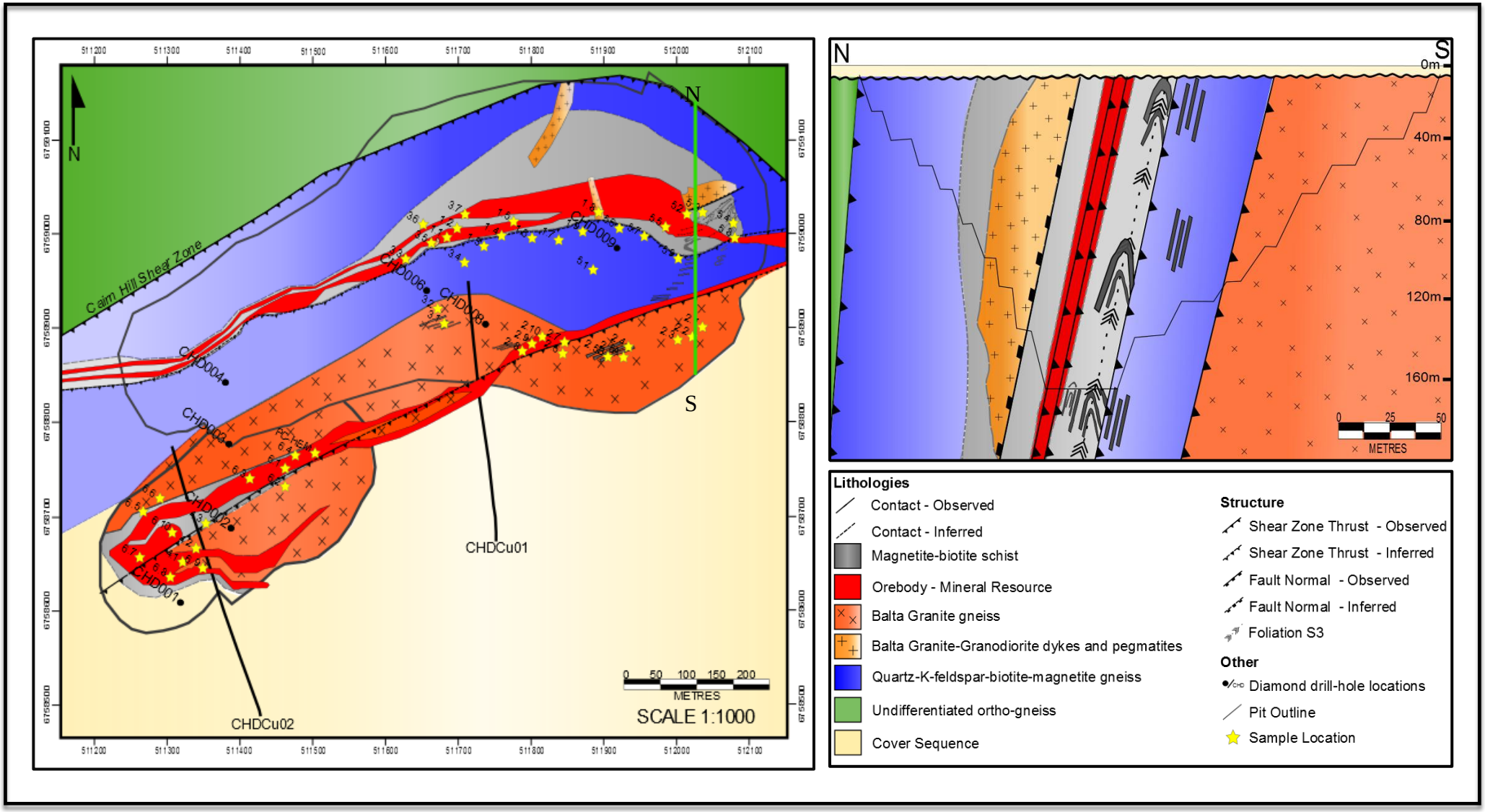

Figure 4: Resultant deposit-scale geological map from field mapping, with accompanying cross-section identifying major lithologies hosting and surrounding the deposit; faults and shear zones are also displayed, including the regional Cairn Hill Shear Zone; along with the orebody in red; collected samples localities are signified by yellow stars; and, lastly diamond drill-hole location accompanied with their coded name.

characterized by clinopyroxene (likely augite), (calcic-) plagioclase, and minor magnetite, amphibole (hornblende) and quartz. The narrow zones characterized by black-green and grey colour are predominantly altered by pervasive chlorite and are highly magnetic (magnetite).

QUARTZ-K-FELDSPAR-BIOTITE-MAGNETITE GNEISS

The predominant lithology hosting the Cairn Hill deposit is a quartz-K-feldspar-biotite-magnetite (QFBM) gneiss and is highly variable with respect to composition, intensity of deformation/strain and alteration. Minor garnet is locally observed within the gneiss. The foliation trends E-SW to W-NE and is coincident with the CHSZ and subsidiary, internal structures. The Cairn Hill deposit is entirely bound to the north, and potentially, also to the south by a similar (if not equivalent) lithotype interpreted to have an igneous protolith. This is, however, poorly constrained within the Mount Woods stratigraphic complex (Chalmers 2007). The Balta Suite granitoids could be a potential protolith.

Locally, the QFBM gneissic fabric preserves rootless-isoclinal folds showing intense fold-limb attenuation sub-parallel to the main fabric; consistent with transposition (S_1 in parallelism with S_2). The QFBM gneiss (and potentially the Balta Suite granitoids) can be recognized as mylonites displaying a penetrative fabric defined by biotite and minor magnetite as metamorphic minerals. Recrystallized quartz-K-feldspar aggregates often appear as rolled clasts occasionally developing interpretable kinematic indicators (delta clasts) providing an approximate E-NE to W-SW trending shear sense correlating well with identified structures within the CHSZ structural corridor.

MAGNETITE-BIOTITE SCHIST

Proximal to and hosting the orebodies is a complex unit comprised of biotite and magnetite, which has a prominent schistosity trending parallel to the regional Cairn Hill Shear Zone (~E-W). Tight isoclinal folding of the lithotype is observed in the eastern wall of Pit 1. It is likely this unit represents a product of Fe-K alteration due to high fluid/rock ratios associated with volume increase in the dilatant CHSZ.

SKARN

Skarn units are among the least abundant lithologies associated with the Cairn Hill deposit forming a narrow zone at depth, only evident in diamond drill-hole CHDCu02. Calcic-skarn is characterised by coarse-grained metasomatic assemblages resembling an exo-skarn and is immediately adjacent a hornblendite (amphibolite), which may represent the regional metamorphic overprint.

Structure

The CHSZ is poorly constrained, however it is interpreted to be overprinted by all regional post- D_2 fabrics and related structures. The F_2 axial plane rotates in complete parallelism with the CHSZ, therefore potentially constraining shear zone formation to the latter stages of the regional D_2 event (Betts *et al.* 2003). Locally, the CHSZ illustrates a contractional duplex in a restraining bend, implicating a positive flower structure (Fossen 2010). The CHSZ is intimately linked with Palaeoproterozoic NW-trending structures, which bound the deposit (Figure 3). Major structures are interpreted to have been reactivated at *ca.* 1450 Ma (Fraser *et al.* 2002).

The gneissic fabric, ore lodes and related shear zones are all orientated sub-parallel to each other, dipping ~70º towards ~170º. The North- and South- ore-lodes are structurally control by brittle-ductile oblique-thrust shear zones. The northern-lode trends 070º and locally shows a 50º clockwise flexure into a 130º orientation, representing a potential local-scale flexural-slip. Consequently, the thickest part of the northern ore lode (40 m width) is located here. This is most likely due to reactivated NW-trending normal faults that bound the Cairn Hill region, potentially causing local structural dislocation. The ore body pinches out/narrows to the east immediately adjacent the dilational jog and becomes barren in copper and gold. The ore lodes have been subject to intense deformation causing development of a strong schistosity and subsequent folding.

Geochronology

Preliminary U-PB SHRIMP analyses on zircons from three representative samples provide upper and lower constraints on the timing of mineralisation (Reid 2013). However, the timing of peak metamorphism is poorly constrained and a potential protolith for the quartz-K-feldspar-biotite-gneiss remains unclear.

Magmatic crystallization age for selected zircons was determined from the Balta Suite alkali-rich granite; however the data was mostly discordant and there produced a poorly defined upper intercept age of 1587 ± 57 Ma (Reid 2013). This age provides a maximum age for early alteration and subsequent mineralisation.

Zircons were selected within a representative sample of the QFBM gneiss, which produced a concordant dataset suggesting an age of 1578 ± 4 Ma (Reid 2013). This age can be interpreted to represent magmatic crystallization.

The cross-cutting granodiorite dyke provided a concordant age of 1525 ± 13 Ma (Reid 2013) thus providing a minimum age for hydrothermal alteration and mineralisation at the Cairn Hill deposit. This age appears to suggest post-Hiltaba phase magmatism although the precise affinity of this event remains unclear. Granodiorites within the region are interpreted to belong to the Hiltaba-equivalent Balta Suite.

PETROGRAPHY

Hydrothermal alteration at the Cairn Hill deposit is largely controlled by the E-NE- to W-SW-trending brittle-ductile faults and shear zones, which represent the locus of copper (-gold) mineralization (Figure 4). Outside the shear zones, protoliths can still be recognized, and hydrothermal alteration primarily depends on the nature of the rock (e,g. predominance of hydrothermal biotite in mafic rocks/gneissic layers compared to hydrothermal K-feldspar in felsic host rocks; Figure 6D and I). In proximal zones, pre-existing features of the host rocks are essentially obliterated and individual protoliths are unrecognizable due to the prevalence of comparable hydrothermal paragenesis in disparate rock units.

Mineral assemblages attributable to hydrothermal alteration are also highly variable from sample to sample, and mineral associations commonly overlap one another. This may indicate a prolonged and possibly cyclic history of fluid-rock interaction, leading to metasomatic and hydrothermal alteration, veining and associated brecciation. The Cairn Hill system involved early emplacement of Balta Suite granitoids (*ca.* 1587 Ma; Reid 2013), closely following a complex evolution encompassing prograde metamorphism/ high-temperature deformation (up to upper-amphibolite facies) and largely coeval hydrothermal alteration.

Early, high-temperature Na-Ca alteration stages are largely preserved in replacement features focused in the Balta Suite alkali-rich granites, distal to the deposit. Younger potassic- and iron- alteration is preserved in veins and as replacement features, proximal to the orebodies (breccias). Copper (-gold) mineralization is coincident with hydrothermal brecciation within K-Fe- altered host rocks between the E-W-trending shear zones that bound the orebody.

A detailed mineral paragenetic scheme (Figure 5) was determined on the basis of cross-cutting relationships among ore veins, mineral assemblages, and ore fabrics identified at macroscopic (field and drill-core) to microscopic scales.

Na-Ca alteration

The earliest alteration event involved intense Na-Ca metasomatism (*cf.* Figure 7), particularly albitization, characterized by assemblages of albite (I) + (meionite-mariolite-) scapolite (I) + Fe-chlorite (I) + diopside (I) + oligoclase + Fe-actinolite/tremolite (I) + (Fe-Mg-)hornblende (I) + hastingsite (± rutile, titanite, magnetite, K-feldspar, pyrrhotite and pyrite). Na(-Ca) assemblages typically occur along (brittle-) ductile (deformation) penetrative fabrics, i.e.. gneissic foliation planes.

Albitization results in white-to-pinkish colour in altered portions of the Balta Suite alkali-rich granite and in QFBM gneiss in distal parts of the deposit (Figure 6g). Albite typically displays chessboard twinning. Albitization is represented by two distinct textures: (i) pseudomorphic replacement of pre-existing (igneous) feldspars (microcline

Mineral	Protolith(s)	Early high-temperature assemblages (600-350ºC)		(Exo-)skarn (600-350ºC)		Retrograde (<350ºC)			Overprint (<100ºC)	
	Pre-alteration	Stage I	Stage II	Stage III	Stage VI	Stage V	Stage VI	Stage VII	Stage VIII	Stage IX
	Primary assemblages	Na-Ca(-Fe) alteration	K-Fe(±Na) alteration	Prograde skarn	Retrograde skarn	Main mineralising event	Late-stage alteration	Regional Metamorphic Overprint	Cambro-Ordovician?	Supergene
Scapolite		marialite		meionite						
Diopside				??						
Ca-plagioclase	andesine	oligoclase								
Garnet				andradite - grossular						
Hornblende										
Actinolite - tremolite										
Hastingsite										
Clinozoisite										
Albite										
Chlorite (Fe → Mg)		Fe						Mg		
Magnetite										
Hematite										
Fluorapatite										
Quartz										
K-feldspar	microcline	orthoclase →								
Biotite (Fe → Mg)		Fe						Mg		
Rutile										
Titanite										

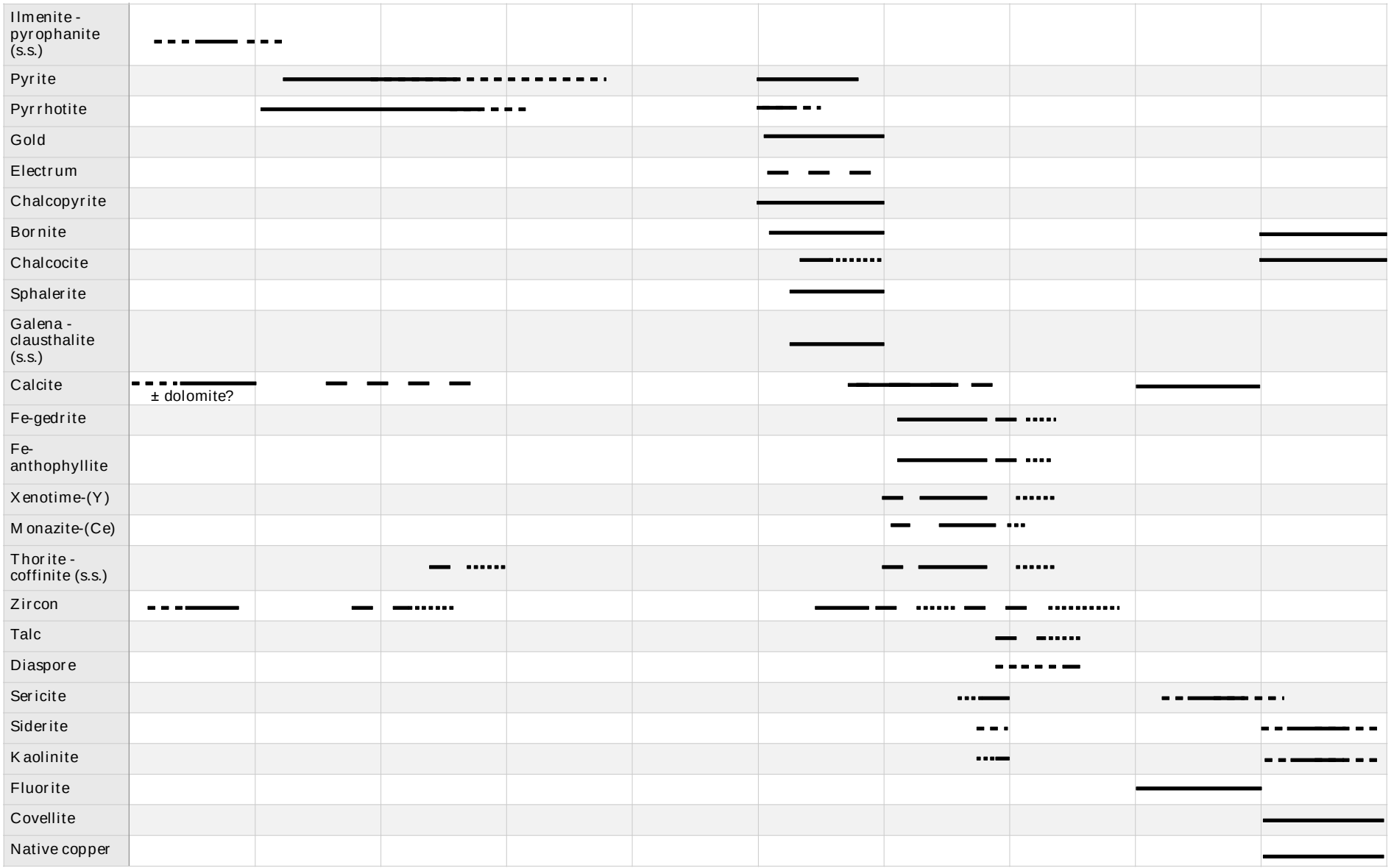

Figure 5: Paragenetic sequence of the Cairn Hill deposit. The sequence is divided into five main stages: (i) protoliths (primary assemblages); (ii) early high-temperature alteration assemblages; (iii) prograde and retrograde (e xo-)skarn; (iv) Retrograde assemblages including mineralisation, post-ore alteration and the regional metamorphic overprint; and, (v) later overprints. Most stages overlap and hydrothermal associations are temporally-, spatially- and chemically-linked to the mineralisation event. Bold to dashed lines represent the relative abundance of each mineral formed in each stage, and confidence of observation, respectively. (s.s. = solid solution; Ce = cerium; Y = yttrium; Fe = iron; Mg = magnesium; Na = sodic; Ca = calcic; K = potassic)

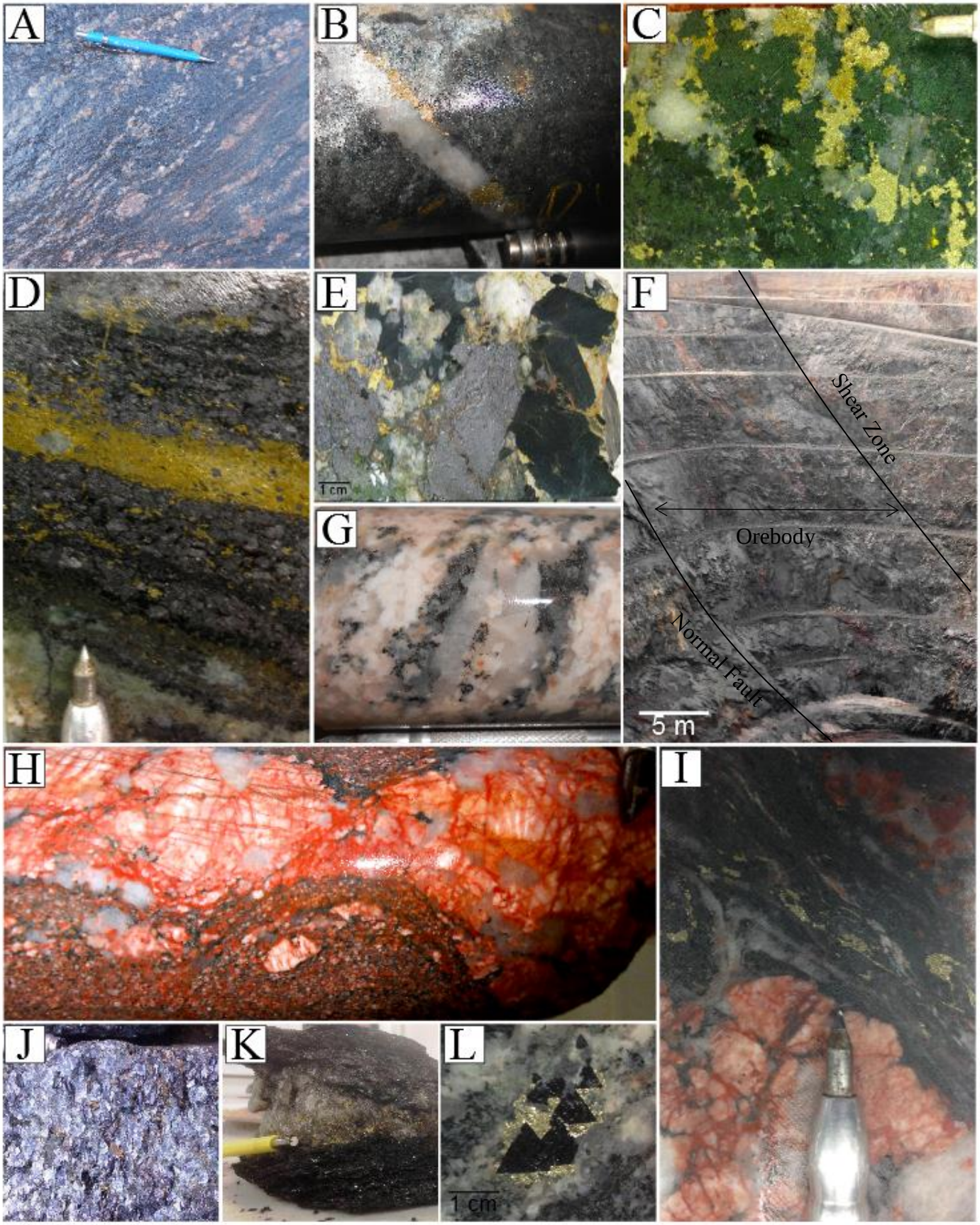
A
B
C
D
E
1 cm
F
Shear Zone
Orebody
Normal Fault
5 m
G
H
I
J
K
L
1 cm

Figure 6: Compilation of images collected in the field located from the Cairn Hill area. Images B-G, H, I and L are representative textures and mineralogy from diamond drill-holes (CHDCu01; 02; and, 03; Figure 4) within Cairn Hill. Images A, F, and J-Lare selected images resultant from the field campaign, involving geological mapping and sample collection. (a) Mylonitized host rock located within the ductile Cairn Hill Shear Zone. Delta clasts are rare, and occurrences are not considered reliable, however some delta clasts provide a ~E-W kinematic indicator validating previous observations. Quartz + K-feldspar clasts show evidence of shearing (rolled clasts) within a milled (fine-grained) biotite ± magnetite matrix typical of a mylonites texture. (b) Magnetite + biotite + amphibole altered matrix, with late (brittle) quartz veining; with pyrite + chalcopyrite evident along the margins. (c) Very typical textures within the Cairn Hill orebody; intimate association between quarts and chalcopyrite-pyrite completely surrounded by green amphibole (likely hornblende) ± magnetite. (d) Brecciated zones, with intense magnetite + biotite alteration with later pyrite-chalcopyrite selectively replacing along the biotite fabric. This is considered to be an earlier relationship with respect to the main mineralisation paragenetic stage. (e) Brecciated orebody with coarse-grained magnetite and hornblende (metamorphic?) crystals within a quartz matrix; pyrite + chalcopyrite overprints these assemblages. (f) Regional-scale view showing the eastern wall in Pit 1, identifying the main shear/fault zones affecting the ore, apparent (isoclinal) folding of the magnetite-biotite (schist) orebody and pegmatitic dyke. (g) Albitite. Typically preserved at depths >400 m within drill-core. Creamy coloured albite is remnant albitization of the host rock, along with minor quartz + biotite + magnetite. (h) Boudinaged quartz + K-feldspar + tourmaline-rich pegmatite, showing a nicely developed shear margin; hosted within a folded clast-rich granitic-gneiss host rock. (i) Relatively coarse-grained granite/pegmatite cut by a magnetite + biotite-rich matrix, overprinted by quartz veins that show marginal folding. Again, pyrite + chalcopyrite is intimately associated with the magnetite and quartz grain margins. (j) Representative image of the (mostly massive orebody) magnetite + biotite ± sulphides schist lithotype. (k) Typical feature on the margin of the Orebody along the shear zone contacts: sschistose biotite ± muscovite with a quartz core, which sometimes hosts chalcopyrite. This is considered a retrogressive metamorphic feature indicating high fluid/rock ratios resulting in remmobilsed Cu to these margins. (l) A rare, nonetheless very interesting texture showing idiomorphic sphalerite (black) with chalcopyrite observed along the contact margins. This provides evidence towards the Cairn Hill hydrothermal system shifting from a ductile regime to relatively brittle, indicated by open-space, infill textures.

and andesine) typified by porous albite containing lamellar intergrowths of commonly seriticized K-feldspar and minor pore-attached hematite in granitoid host rocks (Figure 7e); and, (ii) albite itself can occur as cleavage-orientated lamellar intergrowths predominantly within igneous microcline, but also as blebby intergrowths in igneous oligoclase-andesine (Figure 7f, i and 7j).

Relatively albite-poor calcic-alteration, containing diopside (I), oligoclase, Fe-actinolite/tremolite (I), Fe-Mg- hornblende (I), hastingsite, magnetite (I), pyrrhotite (I) and pyrite (I)), selectively affects primary ferromagnesian minerals in predominantly the QFBM gneiss on the margins, but also within, intensely-altered albitzed zones. Generally, this occurs closer to the orebodies and is concentrated mainly along E-NE- to

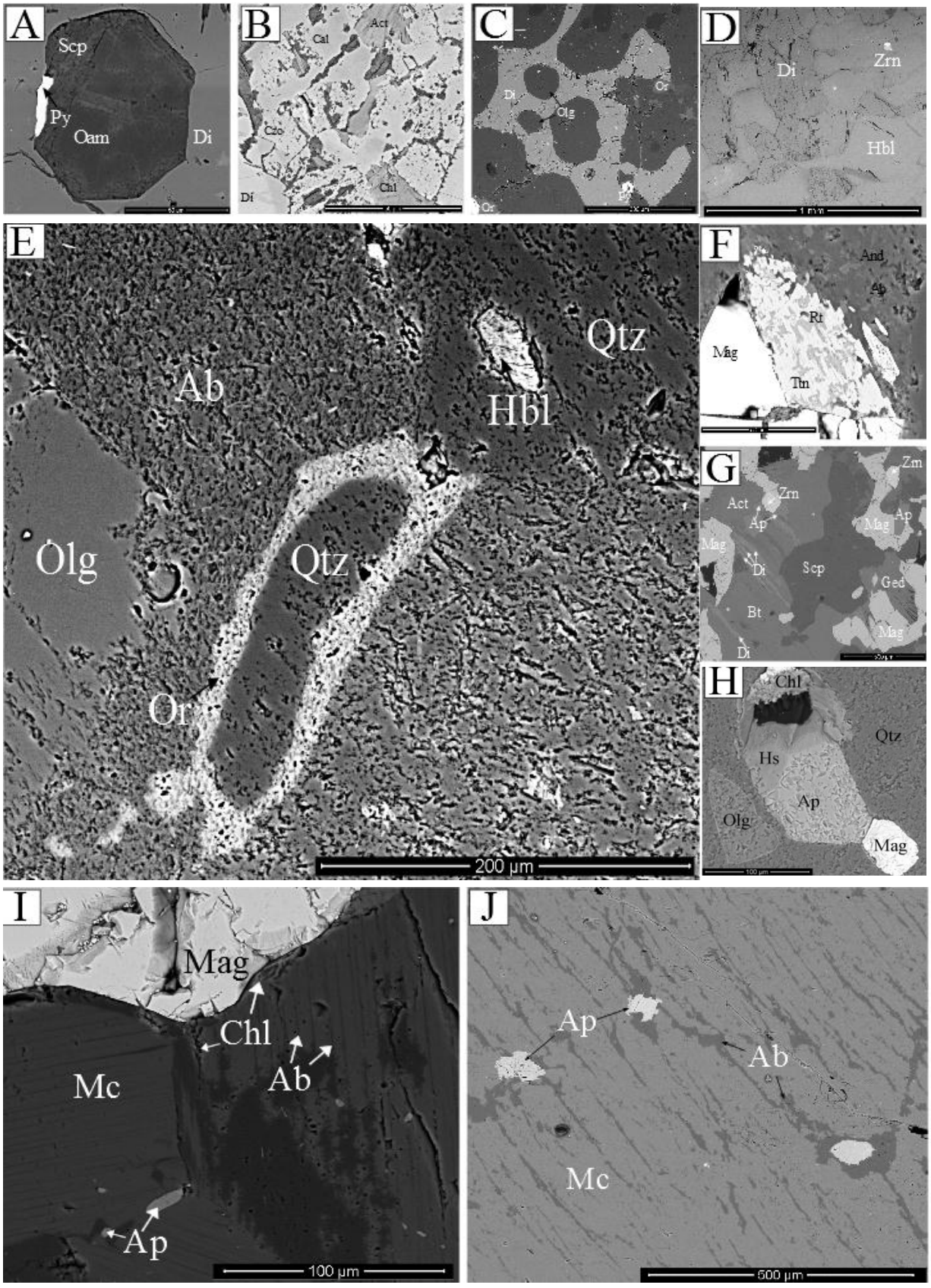
A
Scp
Py
Oam
Di
B
Cal
Act
Cto
Di
Chl
C
Di
Olg
Or
Py
Or
D
Di
Zrn
Hbl
E
Ab
Qtz
Hbl
Olg
Qtz
Or
200 µm
F
And
Ap
Rt
Mag
Ttn
G
Zrn
Act
Zrn
Ap
Ap
Mag
Mag
Di
Scp
Ged
Bt
Mag
Di
H
Chl
Qtz
Hs
Ap
Olg
Mag
I
Mag
Chl
Ab
Mc
Ap
100 µm
J
Ap
Ab
Mc
500 µm

Figure 7: Back-scatter electron (BSE) images showing petrographic aspects of early high-temperature Na-Ca(-Fe) alteration. (a) Pseudomorphic replacement by late-stage Oam of early Scp within a matrix of Di; early Py growth is evident on the Scp margin. (b-d) Calc-silicate alteration typified by coarse-grained Di and Hbl with accompanying Act-Tr and early Chl. Texturally destructive, retrogressed Czo and Cal has affected early assemblages, notably in (b). (e) Concentric texture comprising Qtz rimmed by Or within a pervasive Ab matrix. Paragenetically early, porous Ab has been relatively unaffected (rare) by later potassic alteration. Remnant Hbl is evident within the top-right Qtz grain. (f) Olg-Ab matrix with later Mag being selectively replaced by early Rt and later Ttn. (g) Early Di-Act-Scp assemblage preserved, overprinted by high-temperature Mag + Ap + Bt assemblage. Late, lower-temperature orthoamphibole alteration (Ged) is evident, along with minor Zrn. (h) Early, potentially magmatic Ap, replaced at the margins by minor Mag; both are overprinted by Hs + Chl. Qtz + Olg are evident, and retain the 'porous' features evident in what may have been earlier albitization that has been obliterated. (i and j) Early, cleavage-oriented lamellar Ab replacing primary (magmatic) Mc and Ap. Late Mag growth is evident (i only)
Albite (Ab); orthoclase (Or); andesine (And); oligoclase (Olg);quartz (Qtz); microcline (Mc); fluorapatite (Ap); magnetite (Mag); hematite (Hem); pyrite (Py); biotite (Bt); chlorite (Chl); galena (Gn); pyrite (Py); gedrite (Ged); scapolite (Scp); clinozoisite (Czo); rutile (Rt); titanite (Ttn); calcite (Cal); hastingsite (Hs); actinolite/tremolite (Act/Tr); hornblende (Hbl); diopside (Di)

W-SW-trending shear zones. This spatial association indicates fractures, faults and lithological contacts acted as conduits for the Na-Ca-bearing fluids.

Liberation of K^+ and H^+ from primary minerals into hydrothermal fluids, along with development of minor quartz is a common end-product of early metasomatic processes affiliated with albitization of magmatic feldspars Increasing K+ in fluids drives development of K alteration due to the shift in fluid composition. The antipathetic relationship between areas of Na (±Ca) and K alteration is due to the extensive obliteration, by the latter, of previous albitized rocks and Na-Ca alteration.

Fe-K Alteration

Variably fine- to coarse-grained biotite-rich and magnetite-rich alteration (with rare K-feldspar) overprints early albitized (Na-Ca altered) rocks (Figure 6b and i). Alteration intensity is variable; minor alteration is evident within ferromagnesian-rich rocks/gneiss layers in distal portions of the deposit. However, magnetite-biotite-rich bodies are

focussed along brittle-ductile shear zones proximal to the orebodies, within granitoid and QFBM gneiss host rocks, contributing to strong magnetic anomalies. Fe-K alteration is accompanied with observed K-feldspar (I)-fluorapatite ± pyrrhotite-pyrite-actinolite/tremolite-quartz (*cf.* Figure 8). Such assemblages are observed in places to cross-cut the foliation within the host rock. Granite clasts/blocks are evident within intensely altered magnetite-biotite-rich zones which resemble breccias.

Biotite is commonly observed in altered gabbro dykes, where it primarily replaces augite (clinopyroxene), accompanied by massive magnetite replacement zones and minor plagioclase. However, whether the creamy-white plagioclase represents a primary igneous mineral or is hydrothermal in origin remains unclear. The narrow gabbro dykes

are interpreted to have been intruded quite early in the hydrothermal evolution of the deposit and, in drill-core, are observed to cross-cut both the granitoids and the E-W-trending fabric evident in the QFBM gneiss at depth.

Incipient potassic alteration, represented by K-feldspar ± biotite-magnetite-albite-chlorite-amphibole (actinolite-hornblende), is pervasive throughout the granitoid- and QFBM gneiss- host rocks. Potassic alteration minerals, particularly K-feldspar, obliterate previous mineral assemblages and textures; occurring as vein and fracture infill products and replacement of pre-existing hydrothermal albite-, magnetite-, and biotite (Figure 8a, c and g). Hydrothermal K-feldspar is predominantly distinguished from magmatic K-feldspar by its marked lack of twinning.

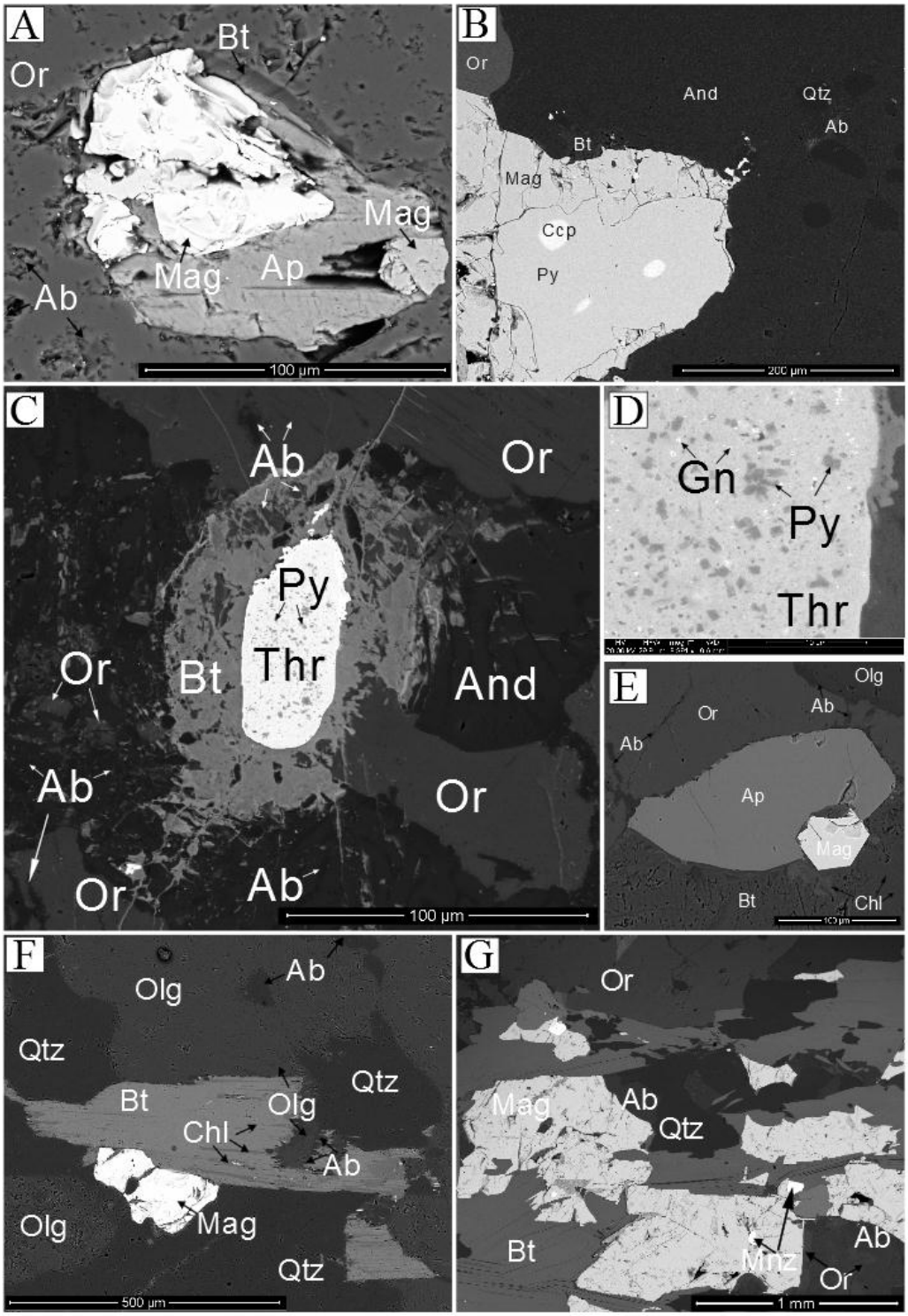

Figure 8: Back-scatter electron (BSE) images showing aspects of K-Fe alteration. (a and e) Early Ap and Mag crystals altered by Or+Bt±Chl; relict Olg and Ab is present. Both images implicate early Mag-Ap±Bt assemblages altered by syn- to later- K-assemblages evidenced by Or±Bt-Chl alteration. (b) Magmatic And replaced by Ab, with minor Qtz inclusions. Later Mag and Or replaces Py, with Ccp evident as "inclusions," it is likely Ccp was trapped during Py growth,. The bleb-like texture of Ccp may relate to the reequilibration of the Ccp during metamorphism. Bt is evident along the margins of Mag and Py. (c) Large grain of Thr replacing earlier Gn (noted in D only) and Py, rimmed by early, higher-temperature assemblages indicative of sodic-calcic to potassic alteration. Early Bt rims around Thr replacing pre-existing Ab and Olg ± Mc; Or represents paragenetically later-stage K-alteration. (d) Detailed image of Thr core, illustrating Py and Gn inclusions within Thr. Gn likely to have formed from radiogenic Pb, a decay product of U within the Thr crystal lattice. S probably sourced from minor breakdown of Py. (f) Ab-Olg (Oligoclase)-Mag matrix altered by later Bt, along with chlorite (Chl) selectively replacing Bt; both minerals overprint Qtz. Re-crystallisation of Ab ± Olg is evident affecting Bt grain. (h) Early albitisation and Mag formation affected by overprinting Or + Qtz assemblage. Bt is observed to form syn-Mag alteration, as it replaces earlier Mag, however is also seen to be replaced by Mag. Minor monazite inclusions are evident in Mag.
Albite (Ab); orthoclase (Or); andesine (And); oligoclase (Olg); thorite (Thr); monazite (Mnz);quartz (Qtz); microcline (Mc); fluorapatite (Ap); magnetite (Mag); hematite (Hem); pyrite (Py); biotite (Bt); chlorite (Chl); galena (Gn); pyrite (Py).

Skarn and amphibolite

Calcic-skarn is constrained to narrow zones interpreted to represent metasomatic replacement of a carbonate protolith, possibly a calcic metamorphic lithology such as dolostone, immediately adjacent to hornblendite (amphibolite). The timing of skarn formation is also poorly constrained. Skarn zones are observed to cross-cut early Na-Ca-K-Fe alteration assemblages. The skarn-amphibolite package may, however, also be relatively early and were possibly unaffected by early alteration stages.

Prograde skarn is characterized by a texturally complex assemblage of garnet (andradite-grossular), scapolite (meionite), magnetite ± diopside. Both the skarn and amphibolite were affected by a retrograde event characterized by development of common clinozoisite, less abundant but widespread actinolite/tremolite, and lesser amounts of titanite, quartz, oligoclase, biotite and chlorite (Figure 11e and f).

Retrograde Alteration

A relatively pervasive retrogressed alteration stage has affected the host rocks, replacing most pre-existing alteration minerals across the deposit, notably chalcopyrite and other sulphides. Retrograde alteration is characterised by assemblages of (Fe-Mg-) chlorite-(Fe-Mg-) orthoamphiboles (anthophyllite-gedrite)-hematite-quartz-calcite which are concentrated within veins (*cf.* Figure 9). Further minerals that may be part of the retrograde assemblage include sericite, talc and diaspore. Together with chlorite, orthoamphiboles represent the most common alteration minerals in all lithologies.

Early retrogressive stages of the hydrothermal system are characterised by a phase of well-developed chlorite alteration, which selectively replaces earlier biotite-, magnetite-

, amphiboles-, and sulphides (Figure 8f; 9a-c and e; 12h). Chlorite alteration accompanies the increased intensity of the mylonitization of the host rocks, typically replacing magnetite-biotite-rich, 'mafic' zones, and resulting in strongly foliated rocks with high chlorite content. Zones of fine-grained grey- to cream-coloured sericite-rich alteration (Figure 10c) are evident, but rare. Sericite-rich zones are associated with narrow matrix-supported breccia with angular to sub-angular fragments of altered host rocks. This breccia type is likely to be associated with brittle fault movement (i.e. fault breccia; Figure 10c).

Replacement of sulphides, predominantly chalcopyrite-, sphalerite-, and pyrite, and also Fe-oxides by orthoamphiboles (gedrite-anthophyllite) is common. Orthoamphiboles appear paragenetically late within this alteration stage and clearly obliterate all previous mineral assemblages identified in the deposit, both proximal- and distal- to the orebodies (Figure 9a, e-f).

The assignation of mineral assemblages to the retrograde alteration stage is somewhat tentative, as a mineralogically-similar retrograde metamorphic assemblage is also prominent throughout the host rocks, particularly along the shear zones. Two individual metamorphic assemblages have been identified within brittle- to brittle-ductile fault zones: (i) perverse calcite **±** quartz; and (ii) common chlorite + epidote-group minerals **±** amphibole-calcite, respectively. Generally, the metamorphic orthoamphiboles, chlorite and biotite are compositionally Mg-rich throughout the deposit, contrasting with the relatively Fe-rich analogues in hydrothermal alteration assemblages.

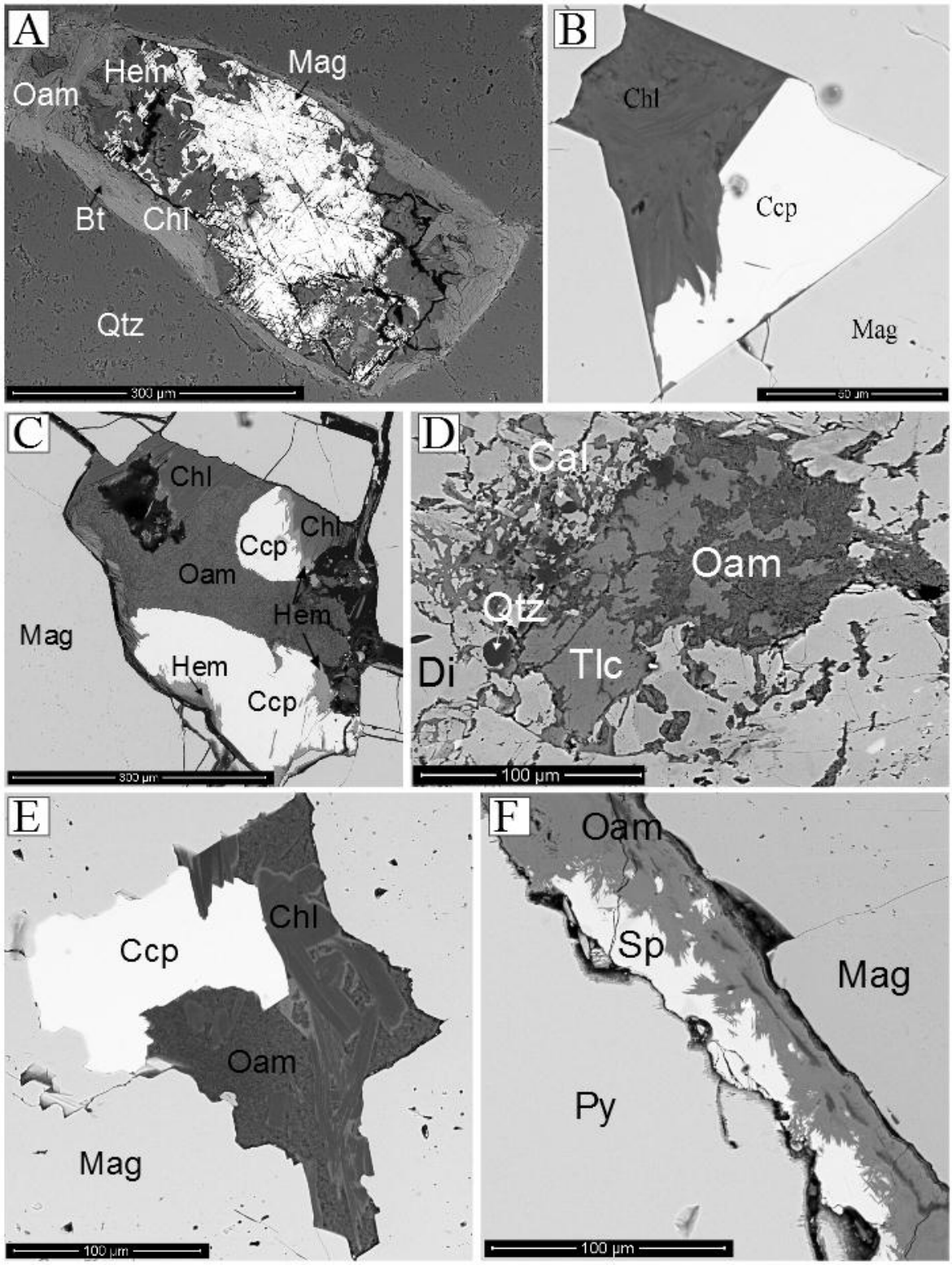

Figure 9: Back-scatter electron (BSE) images representing early low-temperature late-stage (retrogressed) alteration. (a) Typical textures of early assemblages with observed overprinting by later-staged alteration, preserved within granite host rocks. Early Mag+Bt replaced by Chl and Oam within a Qtz matrix. Martitization is evident (pseudomorphic replacement of Mag by Hem). (b-c and e) Typical pseudomorphic textures: replacement of Ccp by Oam (anthophyllite-gedrite) and Chl ± Hem within a matrix of massive Mag. (d) Qtz+Cal alteration within a Di-rich matrix overprinted by rare Tlc and also Oam. (f) Very typical alteration within the Cairn Hill orebody: Massive assemblages of Mag-Py with crosscutting late-stage brittle fractures infilled by sphalerite (Sp) overprinted by Oam.
magnetite (Mag); hematite (Hem); pyrite (Py); sphalerite (Sp); pyrrhotite (Po); quartz (Qtz); calcite (Cal); chalcopyrite (Ccp); orthoamphibole (Oam); biotite (Bt); chlorite (Chl); albite (Ab); oligoclase (Olg); talc (Tlc); diopside (Di); fluorapatite (Ap).

Later Overprints

Bladed hematite, considered to have fomed during a (palaeo-)supergene event, forms a 5-10 m-thick “cap” or “blanket” above the massive magnetite orebodies (*cf.* Figure 10). Secondary chalcocite, native copper, kaolinite, diaspore and abundant carbonates (siderite- and calcite-) appear associated with this supergene event. The timing of this supergene event is poorly constrained, however, and may represent an influx of hydrothermal fluids focussed within the Cairn Hill Shear Zone corridor upon reactivation *ca.* 1450 Ma (Late Kararan Orogeny; Betts *et al.* 2003); this remains equivocal.

A considerably later overprint is evident at Cairn Hill, characterised by a mineral assemblage typical of purple fluorite, accompanied with white quartz-calcite, which generally occur as veins that crosscut the E-W fabric and also ore zones (Figure 10f). This style of overprint may represent a widespread event seen to affect the Olympic Cu-Au Province and is considered to potentially be a product of the Cambro-Ordovician Delamerian Orogeny (*ca.* 515-485 Ma) age (K. Cross pers. comm. 2014). Such an interpretation is however highly conjectural.

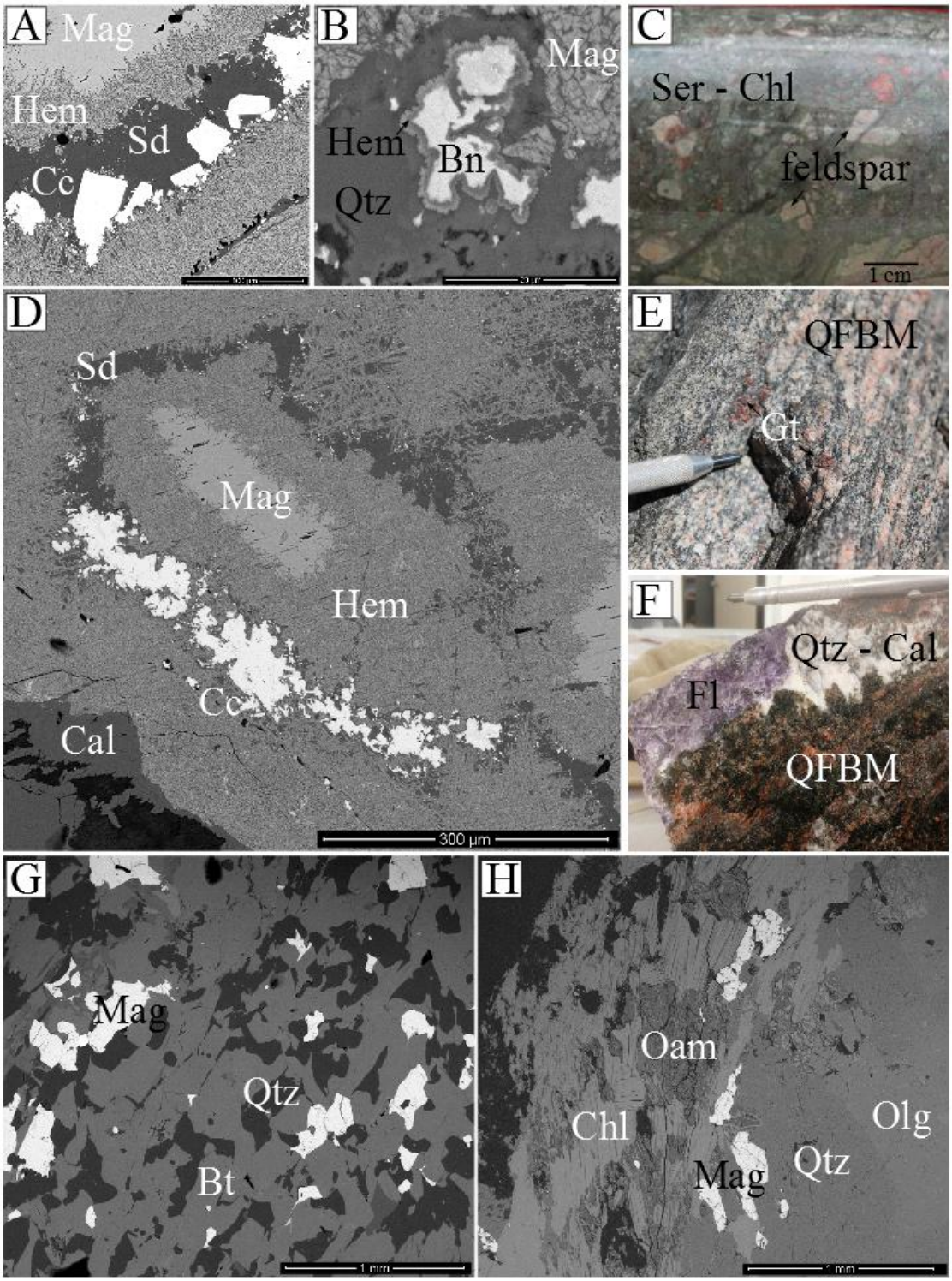

Figure 10: Back-scatter electron (BSE) images (a-b, d; g-h) paired with field images (c, e-f) representing numerous overprinting/later stage alteration phases, including the (palaeo-)supergene event (a-d); Fluorite-calcite-rich overprint (f); and, regional metamorphic overprint (e, g-h). (a-b, and d) Concentric-style, pseudomorphic replacement of Mag by pervasive, bladed Hem (martitization). Cc and Bn are concentrated within Sd-rich alteration zones. Qtz alteration is evident as infill within brecciated, Mag-rich zones (c) Ser-Chl matrix infill within a (fault) breccia suggestive by angular clasts of feldspar (likely K-feldspar + minor albite). (e) Red (grossular) garnet within the QFBM gneiss, selectively forming along ferro-magnesian-rich layers. These garnets are considered to be of metamorphic origin. (f) Fl + Cal + Qtz-rich vein/pervasive replacement of a sample of QFBM gneiss; this overprint is quite rare. (g-h) Bt + Chl + Qtz + Oam with accompanying Mag + Olg is interpreted to represent the regional metamorphic overprint. These assemblages have a well-defined schistosity and overprint all hydrothermal alteration assemblages.
quartz (Qtz); biotite (Bt); chlorite (Chl); magnetite (Mag); orthoamphibole (Oam); oligoclase (Olg); fluorite (Fl); calcite (Cal); garnet (Gt);hematite (Hem); siderite (Sd); chalcocite (Cc); bornite (Bn); sericite (Ser).

MINERALOGY

Magnetite is the predominant hypogene Fe-oxide, and is also the most abundant mineral across the deposit. Magnetite was generated during most stages, from magmatic, regional albitization and K-alteration, as well as the main mineralizing stage. Two distinct generations of magnetite are, however evident: (i) early, high-temperature fine-grained magnetite alteration replacing mafic layers along ductile fabrics; and, (ii) brittle, typically breccia-hosted, coarse-grained magnetite intimately associated with overprinting pyrite-pyrrhotite-chalcopyrite blebs and veinlets.

Hematite is less abundant and is commonly localised along fractures or grain boundaries within the orebodies. Hematite occurs as an alteration product after magnetite. This martitization of pre-existing magnetite is interpreted to have taken place in the latter stages of the main mineralizing event (Figure 9a-d; 11a-c). Hematite is also observed to replace pyrite and chalcopyrite, and is also seen as fracture infill within brecciated zones of the massive magnetite-rich orebodies (Figure 9c; 12a-b, and d).

Incipient magnetite-pyrrhotite is evident disseminated throughout most host/alteration packages, predominantly in the form of veinlets, indicating a shift from a ductile to brittle deformation regime. Pyrite commonly replaces pyrrhotite forming zonal replacement textures within individual pyrrhotite grains, indicating a shift towards more oxidizing conditions (Figure 12b).

Pyrite is associated with chalcopyrite and occurs as infill products within brittle fractures and along grain boundaries, particularly between quartz and magnetite (Figure

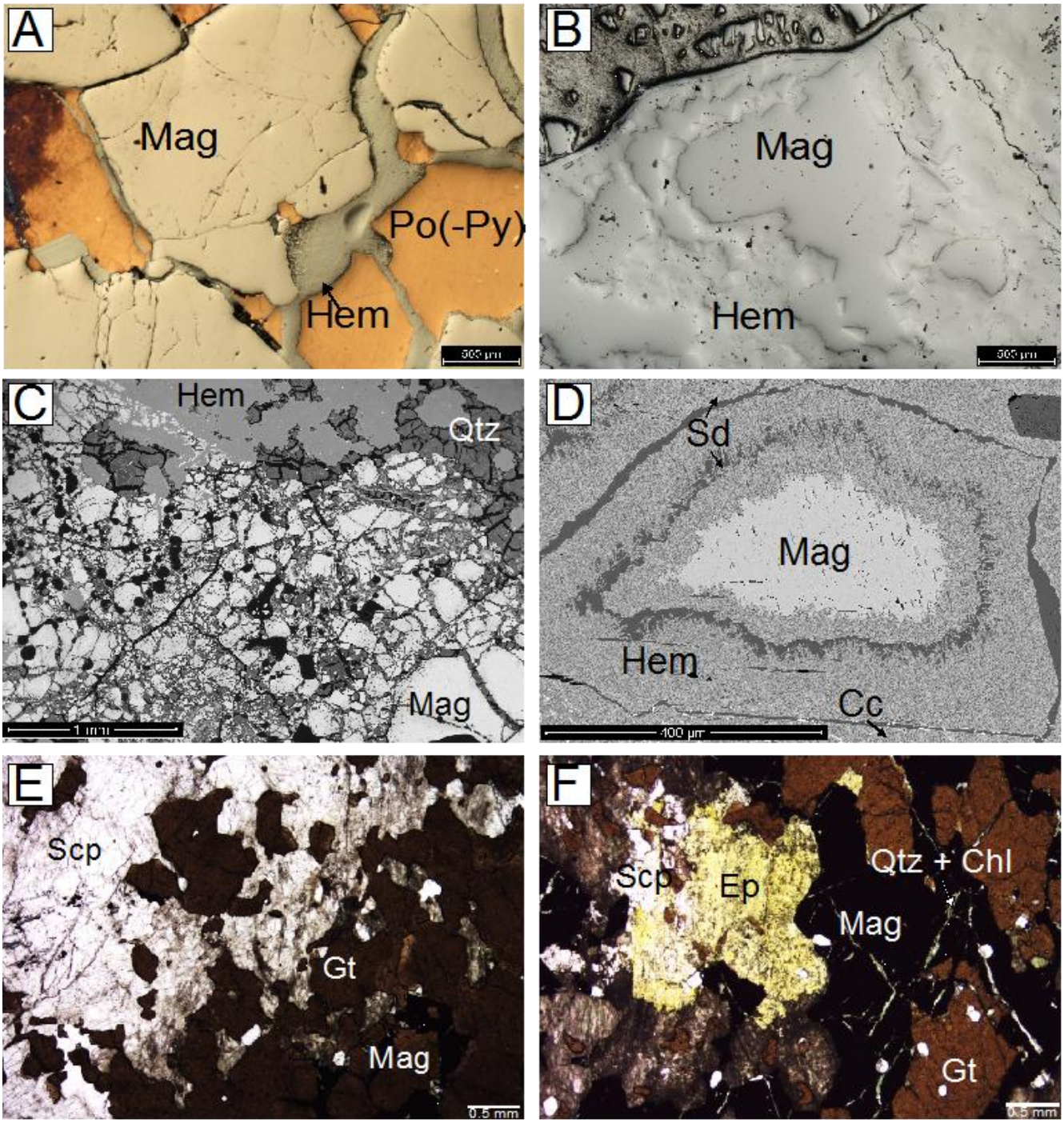

Figure 11: Reflected-light photomicrographs (a-b), back-scatter electron (BSE) images (c-d) and transmitted photomicrographs (in plane polarized light; E-F) showing textures and relationships among iron oxides in the ore zones (a-d) and skarn (e-f). (a) Coarse-grained Mag crystals within later Po-Py matrix, and with Hem rims on magnetite and infilling fractures. (b) Hem selectively replacing coarse-grained Mag (martitization). (c) Strongly brecciated Mag with pervasive Hem alteration; Hem and Qtz define matrix material (d) Concentric texture in which bladed Hem pervasively replacing coarse-grained Mag with Sd infill along fractures, where well-developed secondary Cc is also evident. (e) Contact between Gt-Mag-rich domain and Scp-dominant zone in prograde skarn. (f) Microcrystalline, yellow Ep replacing Scp adjacent to intergrowth of brown Gt and opaque Mag. Qtz + Chl occur as fracture infill within Mag. Ep + Qtz + Chl represent some minerals associated with retrograde skarn. magnetite (Mag); hematite (Hem); pyrite (Py;)garnet (Gt); epidote (Ep); quartz (Qtz); chlorite (Chl).

Furthermore, pyrite and particularly chalcopyrite illustrate a strong spatial association with brittle quartz veining and brecciation, and also disseminated magnetite proximal to massive magnetite ore-lodes (*cf.* Figure 12).

Rare zones of more massive chalcopyrite are observed along margins of idioblastic sphalerite (Figure 6l). Generally, sphalerite predominates over galena and both occur as infill products within micro-fractures, mostly in pyrite, and/or as infill along grain boundaries of pyrite and magnetite (Figure 10a and e). Intermediate members of the galena-clausthalite (PbS-PbSe) solid solution series are common. Most sphalerite and associated galena is, however, observed to be paragenetically later than the main Cu-Au mineralizing event.

Chalcopyrite is the dominant hypogene Cu-mineral in the deposit and commonly occurs within veinlets that cross-cut massive magnetite-apatite-biotite bodies within brittle-ductile shear zones (Figure 6d; *cf.* Figure 12). Bornite commonly replaces chalcopyrite at grain rims (Figure 10c). Late fractures within the bornite-rimmed zones are the products of volume change during replacement; minor secondary chalcocite is observed along these fractures (Figure 10c). Less abundant hypogene chalcocite is evident only at depth and was observed only in diamond drill-core.

On the margins of the massive magnetite-rich orebodies, wide zones of quartz ± platy biotite-muscovite follow the strike of the body and associated shear zones (Figure 6k).

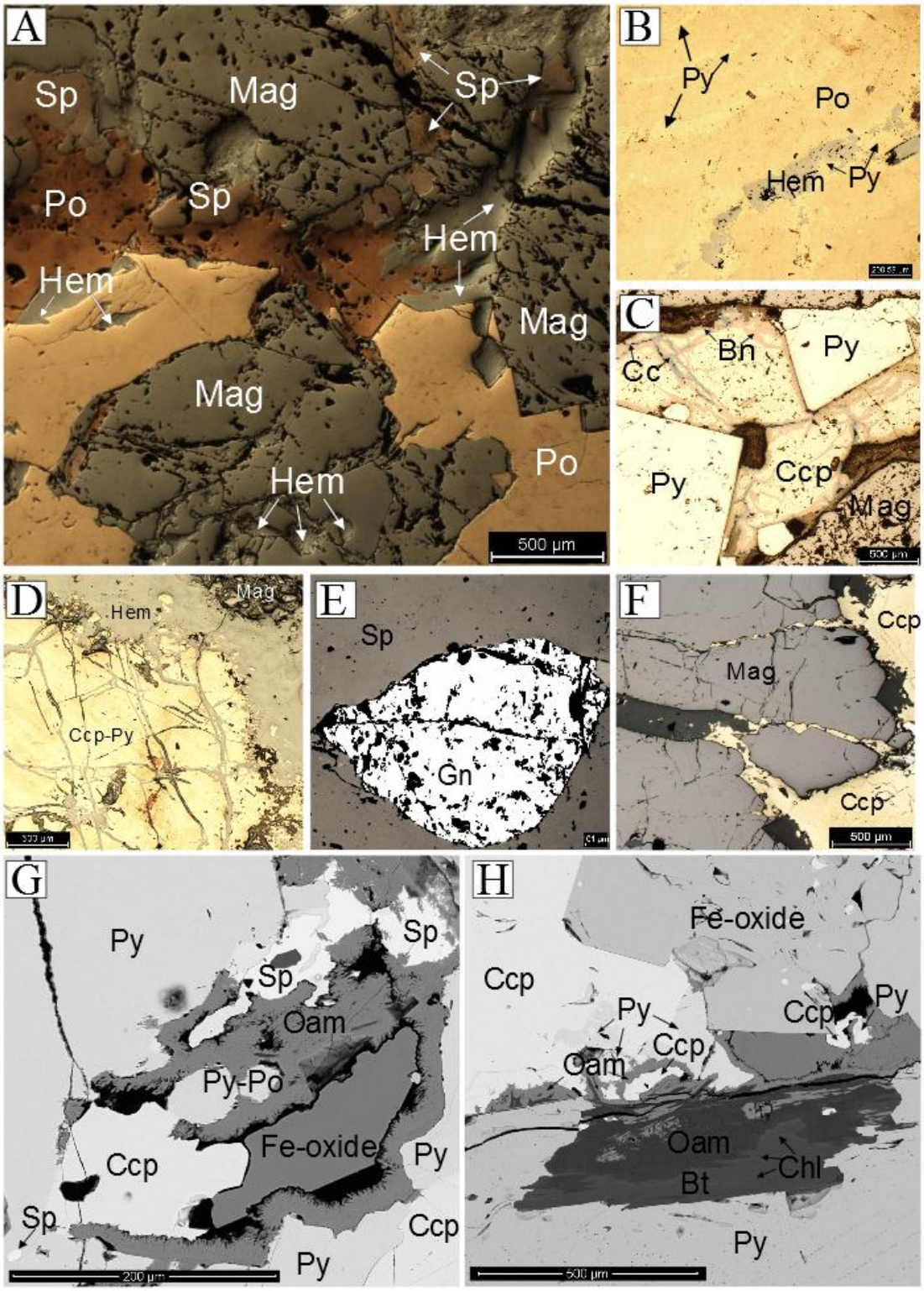

Figure 12: Reflected-light photomicrographs (a-f) and back-scatter electron (BSE) images (g-h) showing petrographic aspects of the main mineralisation stage. (a) Early Mag-Po assemblage overprinted by Hem and Sp alteration representing the paragenetic association of the main mineralisation stage. Minor Py is evident within Po, interpreted to have exsolved from the host during later-staged retrograde stages. (b) Exsolution of Py within pre-existing Po; Hem selectively alters Py. (c) Typical idiomorphic Py grains surrounded by chalcopyrite (Ccp), which is in turn rimmed by Bn. Cc within fractured zones in Bn is likely secondary. (d) Mag and later Ccp (with intergrowths of Py) pervasively altered by Hem. (e) Inclusions of Gn within coarse-grained Sp, Cairn Hill ore-zone. (F) Typical coarse-grained "massive" Mag with fractures infilled by Ccp and later Oam alteration. Fracturing of pyrite provides the foundation for late Hem infill ± Ccp-Oam-Bn (f-g) Early coarse-grained Po-Py and iron-oxide (Mag-Hem) surrounded by Ccp and later Sp, in turn overprinted by late-stage Oam alteration; (most likely anthophyllite-gedrite).
magnetite (Mag); hematite (Hem); pyrite (Py); sphalerite (Sp); pyrrhotite (Po); bornite (Bn); chalcocite (Cc); chalcopyrite (Ccp); orthoamphibole (Oam); biotite (Bt); chlorite (Chl); galena (Gn).

These are interpreted to represent the products of interaction (at high fluid/rock ratios), with retrogressed fluids concentrated in the (hydrous) shear zones. Abundant chalcopyrite ± pyrite occurs within late veinlets and blebs along contact margins within these quartz-rich zones (Figure 6k). The timing of this hydrous alteration is unclear, however, it may represent a late metamorphic product resultant from reactivation of the Cairn Hill Shear Zone.

Minerals containing U, Y and in particular LREE, are relatively abundant throughout the host rocks and are interpreted to have been precipitated from hydrothermal fluid in the late stages of the main mineralizing event and early retrogression. LREE-hosting minerals include thorite, monazite-(Ce), and xenotime-(Y), and are evident across the deposit. They are most abundant within host rocks proximal to the orebodies. Thorite, in places, hosts microscopic inclusions of pyrite and galena; this is, however, restricted to relatively early thorite grains in the overall evolution of the hydrothermal system (Figure 7C and D). Galena inclusions are interpreted to have formed via radiogenic Pb released from decay of ^{232}Th and ^{238}U, coupled with the break-down of pyrite, providing a source for S. Intermediate members of the thorite-coffinite-xenotime-(Y) ($ThSiO_4$-$USiO_4$-$YSiO_4$) solid solution series are common (Figure 13a-b). Xenotime-(Y) is spatially associated with pyrite, the implications of this are unknown, and may be coincidental. Generally, xenotime-(Y) develops along the grain margins of thorite (Figure 13c-d).Monazite-(Ce) is evident in all host rocks forming microscopic inclusions within the matrices of porous albitization and within fluorapatite (Figure 13f-h). Monazite-(Ce) is spatially associated with the breakdown of magmatic. Hydrothermal fluorapatite occurs as inclusions and/or along monazite rims.

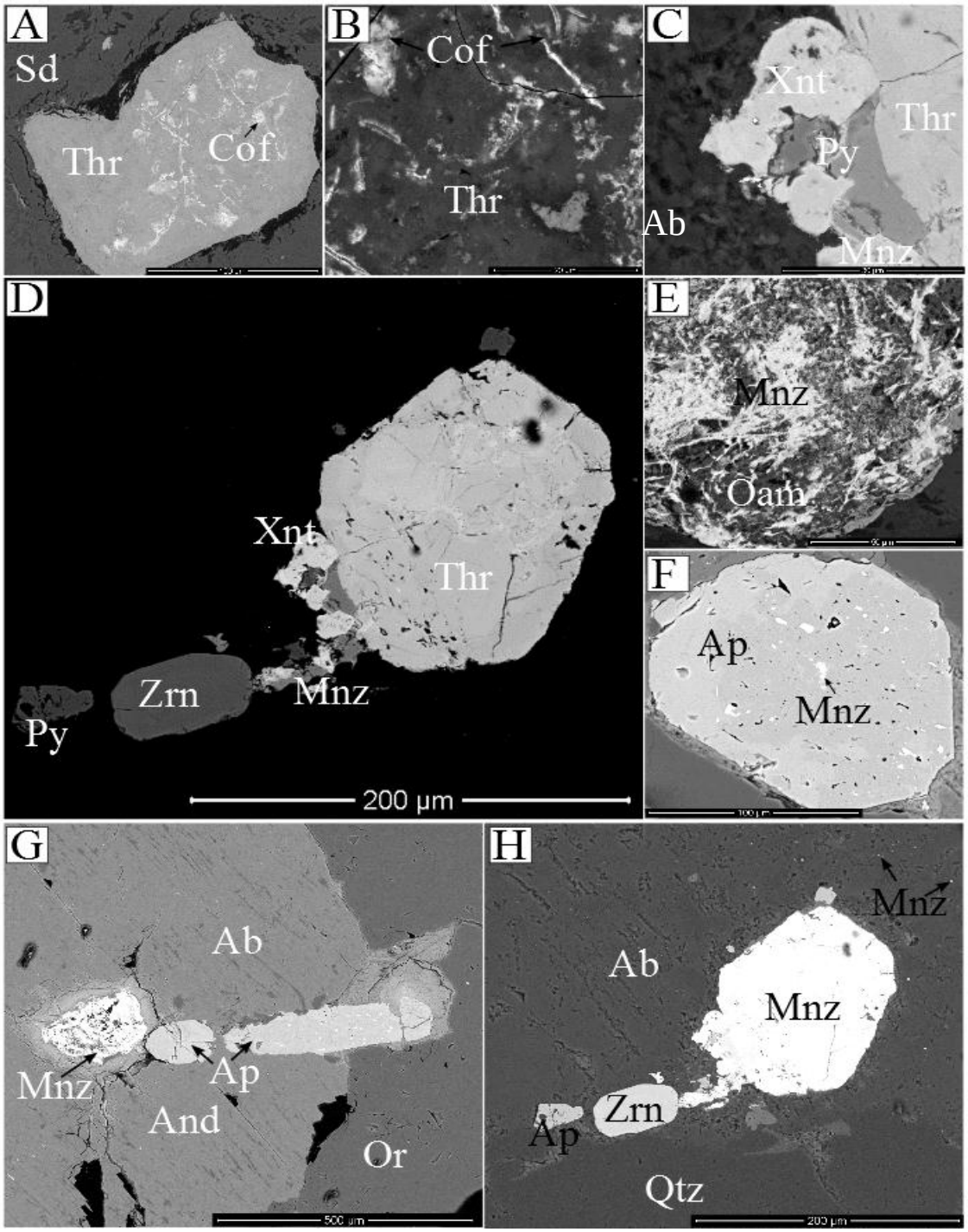

Figure 13: Back-scatter electron (BSE) images representing accessory phases at Cairn Hill. (a) Siderite enveloping and breaking down large Thr grain; compositional differences are evident within Thr – the presence of U-rich portions indicates decomposition o intermediate-member thorite-coffinite ($ThSiO_4$-$USiO_4$) solid solution series. (b) Detailed image of Cof exsolving out of the Thr, noted in (a). (c) Intimate association between Py, Xnt-(Y) and Mnz-(Ce), adjacent a later, large Thr within albitized matrix. (d) Reinforcing the close relationship between Xnt and Mnz-(Ce) adjacent to a hydrothermal/metamorphic (zoned rims evident) Zrn and large Thr. Minor Py is evident. (e) Large Mnz-(Ce) pseudomorphed by pervasive Oam alteration, a common feature expressed within later-staged retrograde alteration. (f) Early, potentially magmatic, Ap with abundant Mnz-(Ce) inclusions. Coloured zonation within Ap represents a Ca-rich rim paired with a Ca-poor core; this may be suggestive of a hydrothermal overgrowth. (g) Early Ap + Mnz-(Ce) affected by minor Chl along the rims, within early albitized And, adjacent later hydrothermal potassic feldspar (Or). (h) Again, early albitization is evident, with minor (magmatic?) Ap broken down consequent of the early alteration. Large Mnz-(Ce) pseudomorphing pre-existing Ap, associated with adjacent Zrn. Zrn shows minor zonation, indicating a potential hydrothermal or metamorphic origin. Mnz-(Ce) inclusions are evident within the porous albite matrix.
Thorite (Thr); coffinite (Cof); pyrite (Py); xenotime (Xnt); monazite (Mnz); zircon (Zrn); fluorapatite (Ap); albite (Ab); andesine (And); orthoclase (Or); quartz (Qtz)

DISCUSSION

Ore Genesis

The CHSZ represents a complex evolution involving both syn-hydrothermal alteration and syn-deformational metamorphism at amphibolite facies. Progressive exhumation resulted in temperature and pressure decreases under high-fluid pressure causing the CHSZ to cross the brittle-ductile transition. This occurred relatively late in the hydrothermal-metamorphic evolution, resulting in a contractional duplex in a restraining bend suggestive of a positive flower structure (Fossen 2010). Dilation during deformation thus strongly concentrates fluid flow. The E-NE to W-SW-trending CHSZ and subsidiary shear/fault zones played a critical role in focussing hydrothermal fluids and provided effective pathways for upward migration of fluid, and also promoted high fluid/rock ratios. The subsidiary shear zones provided local controls on the morphology of the massive magnetite bodies which host the Cu-(Au) mineralisation. The variably mylonitized rocks hosting the orebodies show flexural slip, implying thrusting along layer interfaces during folding causing zones of high strain, which in turn act a reliable fluid conduits (Fossen 2010).

The origin and sources of ore metals is not unequivocally established. However, the deposit is spatially and temporally associated with Hiltaba Suite granitoids, which potentially provide heat, magmatic-hydrothermal fluids exsolved during crystallization of volatile-rich granites and also a potential source for metals (Cu-Au). Reactivated, potentially deep, mantle-tapping Palaeoproterozoic NW-trending faults intersect the CHSZ and play a fundamental role in concentrating Hiltaba Suite magmatism (Haywood & Skirrow 2010). In addition, regional (hyper-)saline metamorphic brines

may also play an integral role in sourcing, concentrating and precipitating metals. A comprehensive fluid-inclusion and/or stable isotope study would be required to resolve potential sources of ore metals and sulphur. Although this was beyond the scope of this paper, a potential model for ore genesis can be given.

Hydrothermal alteration systems resultant from a single fluid pulse preserves the earliest alteration within the fluid conduit, with later stages advancing outwards this zone (Reed, 1997). In contrast, the complex, often overlapping phases of alteration and their spatial zonation point to a protracted evolution of the hydrothermal system. Distal to the orebodies, a regional halo encompassing incipient, high-temperature Na (-Ca) alteration, particularly albitization is evident, affecting the alkali-rich granitoid- and the QFBM gneiss host rocks. Na (-Ca) alteration is practically obliterated by overprinting magnetite-biotite-rich alteration and subsequent K-feldspar. Early metasomatic processes were largely controlled by the mineralogy and permeability of the host rocks and are suggestive of relatively low fluid/rock rations. Proximal to the orebodies, pervasive chlorite ± amphibole alteration accompanied by quartz veining is abundant, indicating higher fluid/rock ratios and a shift to a brittle environment.

The temporal evolution of the hydrothermal system indicates a shift in physicochemical parameters, controlling metal precipitation (Figure 14). Incipient Na(-Ca) alteration is considered to have formed by immiscible separation (unmixing) of H_2O-CO_2-NaCl ± $CaCl_2$-KCl from magmatic fluids into a hypersaline brine with accompanying CO_2-rich vapour (Pollard 2001). This results in a hydrothermal fluid in equilibrium with albite at high-temperatures (Pollard 2001). A magmatic-hydrothermal genetic link to albitization

implicates that associated alteration assemblages were formed at temperatures exceeding 500-600 ºC (Oliver 2004; Pollard 2006). This is consistent with formation of marialite (Na-scapolite) during this stage, (>400-500 ºC at 2-3 kbar; Vank & Bishop 1982). Marialite formation is controlled by high NaCl ± H_2O content within hydrothermal fluid (Vank & Bishop 1982). Furthermore, marialite occurrence reflects buffering of chlorine activity, which may be attributed to regional migration of hypersaline brines. Migration results in metal (Cu, Au, Fe) leaching from host rocks (e.g. Hiltaba Suite granitoids and gabbro) and metal transport as chloride complexes.

Na (-Ca) metasomatism occurs in response to fluid-rock interaction by processes of diffusion, dissolution and re-precipitation (Kontonikas-Charos *et al.* 2014). Typical replacement of igneous feldspar by Na-bearing minerals (albite, scapolite), paired with chloritization of biotite, liberates K^+, H^+, Fe and minor sili*ca.* This progressively lowers the pH of hydrothermal fluids and drives K-alteration. Fluctuations in fO_2 due to fluid-rock interaction control biotite precipitation. Iron is highly soluble in high-temperature, saline fluids and at lower pressures and pH (Williams 1994). Albitization also acts as a driving force with respect to increasing Fe solubility, due to increasing H^+ in the system, resulting in large Fe fluxes. Early magnetite formation is evident due to fluctuating temperatures allowing reaction with suitable host rocks (Williams 1994). Iron is partitioned into early chlorite, amphiboles and sulphides (pyrite-pyrrhotite) indicating saturation of the fluid with respect to S.

Relatively more oxidized and acidic fluids responsible for K-alteration obliterated the early Fe-bearing assemblages, resulting in dissolution of Fe. Pervasive chlorite-

amphibole (green actinolite-hornblende) alteration occurred in zones proximal to the orebodies and overprint earlier Na(-Ca) alteration. Chlorite-amphibole alteration implicates a decrease in pH coupled with a fO_2 increase.

Massive magnetite bodies that formed along the locus of subsidiary shear zones are interpreted as the products of metasomatic processes. Hemley *et al.* (1992) showed that temperature decrease, particularly in the ~500-300 ºC range, results in a dramatic decrease in Fe solubility. Temperature decrease, coupled with increasingly oxidized fluids controlled Fe precipitation as magnetite. Regional circulation of hypersaline metamorphic brines present optimal conditions for enhanced Fe solubility, with associated reactions stripping Fe from local rocks (Williams 1994), indicating potential involvement of a secondary fluid. The magnetite bodies may however represent products of a palaeo-metasomatic process that resulted from an earlier orogenic/metamorphic event. Alternatively, the magnetite bodies may represent recrystallised, Palaeoproterozoic BIF units, with an overprinted hydrothermal event resulting in Cu (-Au) mineralisation. Large bodies of Fe-oxides represent redox buffers that can trap migrating ore-forming fluids.

Quartz deposition was likely controlled by changes in physico-chemical parameters, particularly decreases in pH, temperature and salinity that reduce silica solubility (Fournier 1983). Early deformed and brecciated quartz-rich veins and zones were likely influenced by mixing of high- and low-salinity fluids, promoting quartz precipitation. Such fluids could be the products of mixing between saline fluids of metamorphic

and/or magmatic origin with lower-salinity meteoric fluids descending through shear zones.

Early pyrrhotite deposition requires low fO2 and fS2 (cf. Figure 14) indicating reduced conditions, compared to later pyrite deposition, often replacing pyrrhotite, which requires more oxidized, higher fO2 and fS2 (and/or lower temperatures). Introduction of Cu and Au into the system may not necessarily coincide with precipitation of Fe. Early hypersaline fluids responsible for earlier alteration likely contained Cu and Au in solution as chloride complexes, however did not precipitate due to unsuitable conditions or lack of sulphur. The deposit shows widespread evidence of sequential phases of alteration and also a late brecciation of the magnetite bodies. The brecciated magnetite bodies may represent a potential trap for Cu-Au (± other base metals), indicating a strong redox (fO2) control on metal deposition. Chlorite-amphibole alteration and subsequent quartz brecciation and veining both post-date Na-(Ca) alteration and are intimately associated with the Cu-Au mineralisation. Precipitation of chalcopyrite is considered to have occurred relatively late in the hydrothermal system, spatially associated with quartz brecciation and veining overprinting massive magnetite bodies. Minerals associated with chalcopyrite, representing the 'main mineralizing stage' are characterized by textures suggesting open-space infill and brittle fracture networks. The evolution of such textures are typical of ore deposition at <350-300 ºC and ~1.5 kbar (Seward & Barnes 1997; Figure 14).

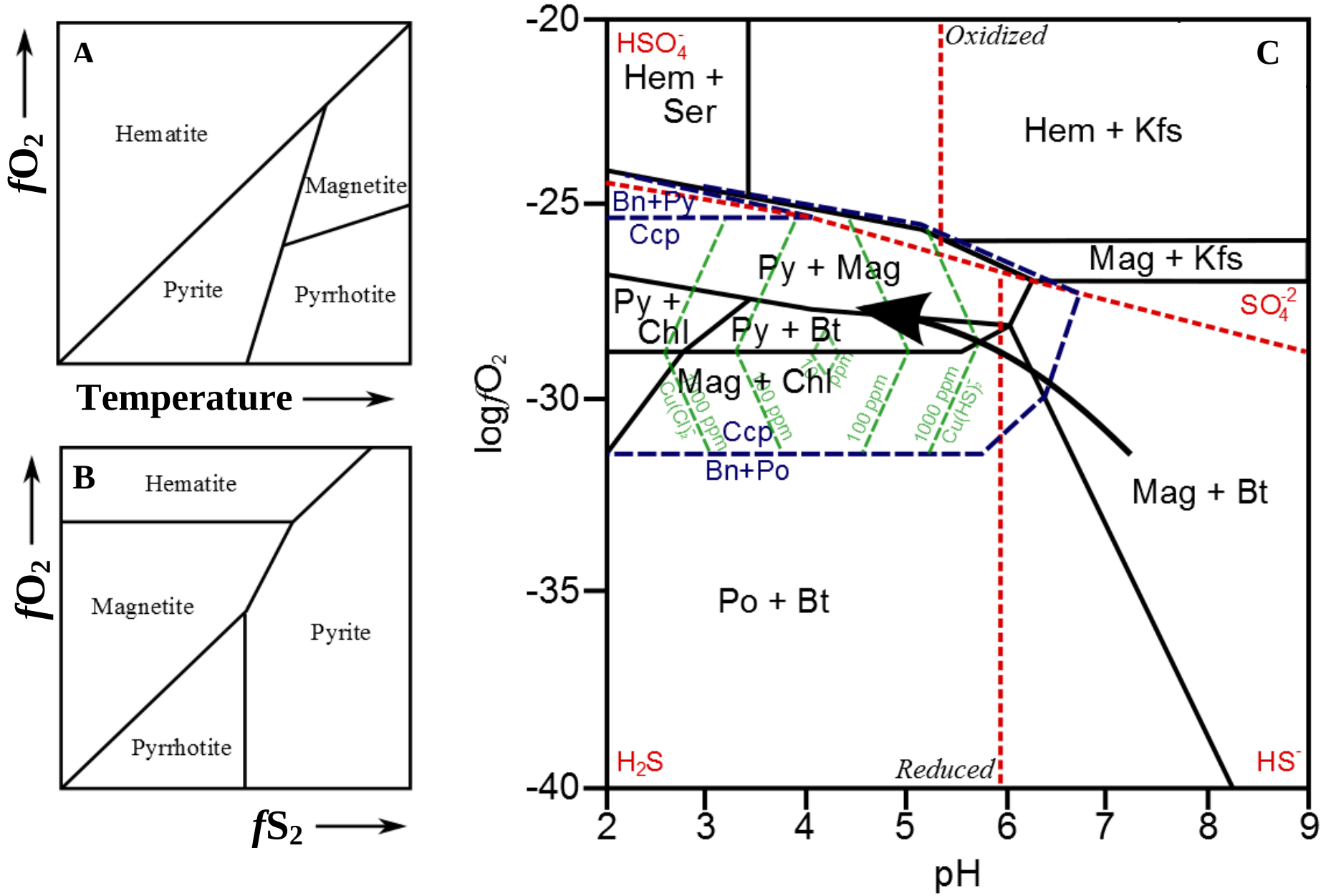

Figure 14: (a-b) Stability relationships in the system Fe-S-O in terms of temperature, fO2 and fS2. C: Approximated diagram of relationship between pH and fO2 at temperatures <350-300 C and 1.5-4 kbar, showing the possible evolution of pH and O2 of the mineralising fluid (arrow) from initial, higher-temperature reduced conditions to later, lower-temperatures, oxidized conditions (copper-bearing paragenesis). (a-c) Adapted from Rotherham (1997)

The paragenetic evolution of the Cairn Hill deposit therefore indicates progressive changes in physico-chemical parameters. Early, high-temperature (500-400 °C) (scapolite-albite-alteration) to lower-temperature (<350-300 °C) late mineralising veins and subsequent retrogressive alteration accompanied by fO_2 increase and decrease in pH and salinity. Importantly, the hydrothermal system also reflects a change in fluid conditions, and possibly source. Early Na (-Ca) and subsequent K-Fe alteration developed at high-temperatures in response to fluid-rock interaction with circulating hypersaline and metalliferous fluids. Such fluids may have a magmatic-hydrothermal source (although a hypersaline metamorphic brine may have also been involved). Ore deposition was potentially controlled by the interaction with hot, hypersaline metalliferous fluids with focussed, dilute, cooler fluids concentrated within subsidiary shear zones.

Crustal Architecture and Regional Geodynamics

The definition of IOCG deposits has evolved into a highly contentious issue since the deposit clan was introduced by Hitzman *et al.* (1992). This stems from the fact that many deposits have been misclassified due to poor understanding of the range of deposits included. Groves et al. (2010) proposed a modified classification system emphasizing the common features of giant (resources >100 Mt) Precambrian "IOCG *sensu-stricto*" deposits, based on their geological and tectonic settings. IOCG deposits *sensu-stricto* represent the dominant members of the IOCG family and are interpreted to be a continuum of ore systems between end-member deposit styles: deeper, magnetite-rich-; and shallow, hematite-rich- systems (Hitzman et al. 1992; Barton, 2014). End-member deposits are defined by both specific and common characteristics.

'Transitional' IOCG systems are evidenced by the presence of early Na-Ca alteration overprinted by pervasive K (-Fe) alteration (Barton & Johnson 2004).

IOCG deposits *sensu-stricto* within the 1.6 Ga Olympic Cu-Au Province are characterized by both end-members and form a spatial metal zonation across the metallogenic province encompassing 'mesozonal' bounding the northern and southern regions of the province, and 'epizonal' in the center (N. Haywood pers. comm. 2014, D. Groves pers. comm. 2014). Mesozonal deposits such as Cairn Hill or Hillside represent deeper, 'magnetite-rich' systems; whereas epizonal deposits (e.g. Olympic Dam, Prominent Hill) are characterized by shallow, 'hematite-rich' systems.

The genesis of IOCG deposits within the Gawler Craton has traditionally been attributed to development of a mantle plume within an anorogenic, intracontinental setting (Hitzman et al. 1992; Stewart & Foden 2001; Groves et al. 2010). However, Betts *et al.* (2006; 2009) advocate a Mesoproterozoic plume-modified orogenic model, in which the northwards-subducting slab along the southern Australia plate margin interacts with an impinging plume. Heat generated from plume interaction with the down-going slab led to the formation of the Gawler SLIP; which resulted from partial melting of metasomatised SCLM induced by and subsequent ponding at the Moho (crustal-lithosphere) boundary (Groves *et al.* 2010; Betts *et al.* 2009). The implication is that the Gawler SLIP was emplaced in a compressional tectonic setting. Features of the Cairn Hill deposit, notably formation of the hydrothermal system penecontemperaneous with high-temperature deformation and metamorphism support a compressional model.

REGIONAL CONSTRAINTS ON THE SOURCE FOR THE GAWLER SILICEOUS LARGE IGNEOUS PROVINCE

The northwards-subducting slab along the southern Australian plate margin is evidenced by ca. 1620 Ma St. Peters Suite arc magmatism (Swain *et al.* 2008). Elevated intracontinental geothermal gradients due to thinning of the continental crust (i.e. extension in a back-arc basin; Betts *et al.* 2009) are evident. Gradual flattening of the slab, potentially due to subduction of buoyant oceanic lithosphere (causes unclear), results in an intracratonic migration of arc-magmatism due to removal of the asthenosphere wedge (*ca.*1610-1595 Ma; Betts *et al.* 2009). During this process, hydration of the lithosphere, i.e. metasomatism of SCLM takes place, increasing the concentration of volatiles, incompatible elements and ore metals associated with IOCG deposits (Groves *et al.* 2010). Subsequent delamination of the slab exposes the asthenosphere to the fertilized, metasomatised SCLM. Voluminous partial melts are generated, which pond at the crustal-lithosphere boundary. Ponding leads to partial melting of continental crust forming intermediate-to-felsic-large igneous provinces. At this time slab roll-back (*ca.* 1595-1575 Ma; Betts *et al.* 2009) occurs and results in crustal extension also associated with thermal upwelling. This results in an ignimbrite flare-up, evidenced by the Gawler SLIP; modern analogues include the Basin and Range, Nevada, USA.

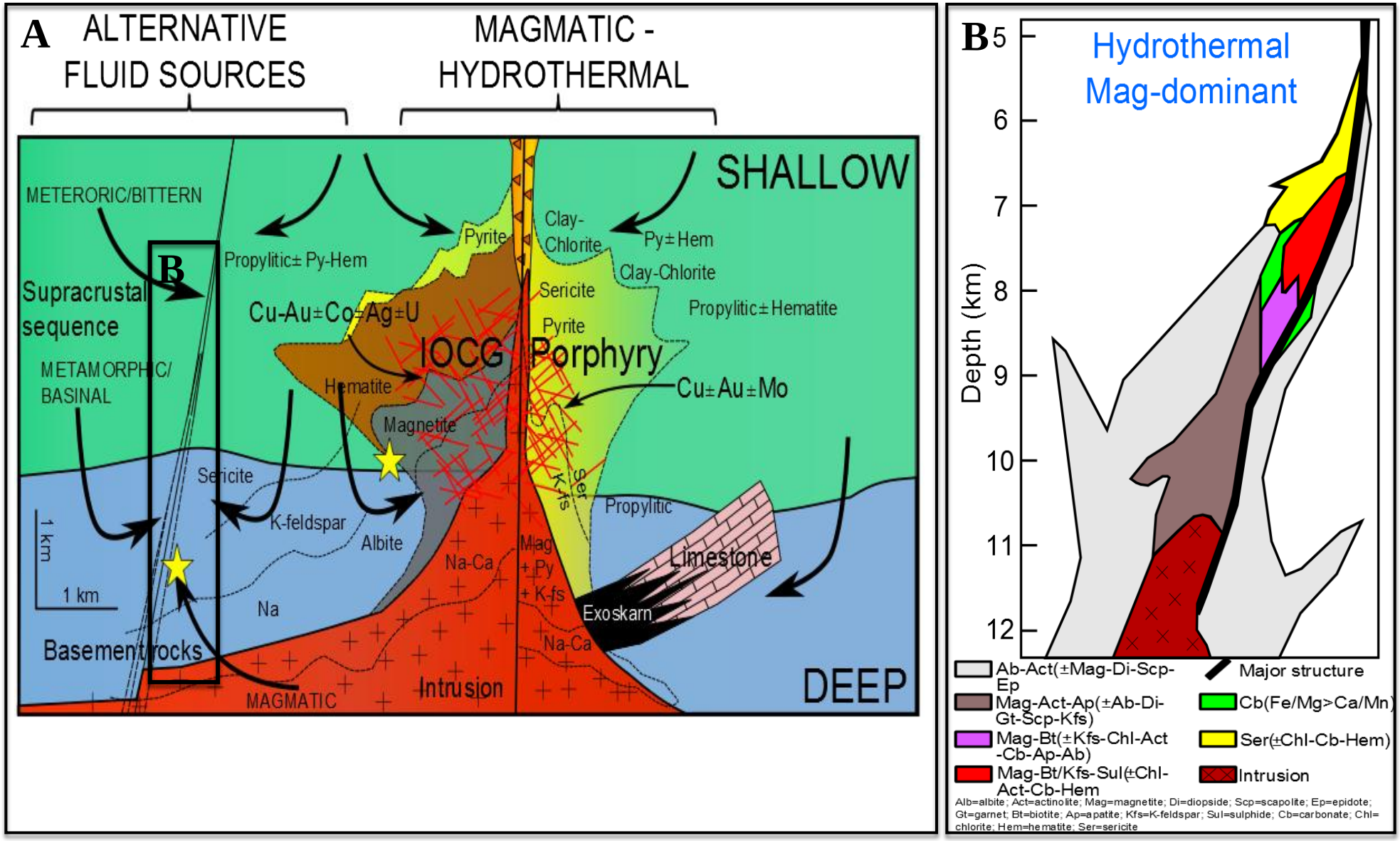

Figure 15: Conceptual ore genesis model(s) integrating magmatic-hydrothermal continuum with alternative fluid sources providing external sources for S (SO4-); resulting in "fluid-mixing" of meteoric/bittern fluids and/or metamorphic/basinal fluids with magmatic fluids producing distinctive hydrothermal alteration haloes and mineralising styles. The two stars indicate Cairn Hill's potential position(s) representing either a purely magmatic-hydrothermal model, or alternatively a fluid-mixing model favoured by most literature with respect to IOCG formation. (a) Adapted from Richard and Mumin (2013) and Williams (2014). (b) Modified after Haywood (2010)

Exploration Implications

Cairn Hill deposit characteristics can be compared to some IOCG systems within the within the Cloncurry District (e.g. Ernest Henry; Eloise; Osborne), the Carajás Province, Brasil (e.g. Sossego; Salobo), and shares features with several prospects within Gawler Craton (e.g. Hillside; Manxman; Oak Dam East). These common characterisitcs relate to formation at deeper crustal levels, and an intimate association between alteration/mineralization and regional metamorphism and accompanying deformation. Shear zones also play a critical role in controlling the distribution of magnetite-rich bodies, which host Cu-Au mineralisation. Cairn Hill may be classed as a 'transitional-style' IOCG system, based on early models of Hitzman *et al.* (1992) primarily due to the occurrence of early Na-Ca alteration overprinted by K (-Fe) alteration.

The MWI represents a relatively under-explored region. Conceptual targeting should focus on wide ~E-W-trending structural corridors, such as the CHSZ, that critically have intersecting NW- to N-NE- trending structures. Regions of structural dislocation, e.g. contractional duplexes in a restraining bend (dilatant zone/jog) provide effective fluid pathways allowing high fluid/rock ratios. The significance of the spatio-temporal association of alteration/mineralization with Hiltaba Suite magmatism is unclear, with deposits across the region often independent of such intrusions. Iron-rich metasomatic processes are widespread in the MWI, therefore regional magnetic surveys represents a poor tool in constraining potential exploration targets.

CONCLUSIONS

- Deposit evolution points to: (i) regional circulation of hypersaline metalliferous fluids; (ii) intense fluid-rock interaction resulting in highly modified lithotypes; and, (iii) evolution of physico-chemical parameters indicate early, high-temperature (500-400 °C resulting in scapolite-albite) alteration to lower-temperature (300 °C) retrogression (late mineralised veins), accompanied by decrease in salinity and pH, and increase of fO_2.
- Overprinting of proximal chlorite-amphibole alteration and silicification resulted from significant influx of dilute fluids within E-W shear zones, which represent effective fluid pathways.
- Minor brecciation and late veins with open-space infill textures potentially indicate progressive exhumation of the hydrothermal system.
- Marked K-Fe alteration suggests a transitional magnetite-to-hematite deposit
- The Cairn Hill deposit possesses common features of a deeper, magnetite-rich end-member IOCG deposit, based upon: (i) strong structural control (ore hosted within brittle-ductile shear zones); (ii) hydrothermal alteration and associated mineralisation are constrained to be relatively coeval with Hiltaba Suite magmatism; (iii) replacement of magnetite by hematite accompanied precipitation of copper mineralisation; and, (iv) proximity to a major magnetic-gravity structure

ACKNOWLEDGMENTS

I would like to thank IMX Resources and DSD for their financial support. In-particular Adrian Fabris (DSD) for his help in interpreting the regional geology and countless discussions. Peter Hill (IMX Resources) for his help, reliability, resourcefulness and enthusiasm for this project. A special thanks to my supervisor Nigel Cook for his endless efforts and support throughout the year, I could not have completed this project without you. I would like to acknowledge IMX Resources and various consultants for the additional structural and mapping data required for this thesis, due to accessibility constraints within the mine. Thanks are owed to my fellow Honours colleagues for their moral support. The staff at AM, especially Ken Neubauer for guidance in operating microanalytical equipment.

REFERENCES

ALLEN, S.R., MCPHIE, J., FERRIS, G., AND SIMPSON, C., 2008, Evolution and architecture of a large felsic igneous province in western Laurentia: The 1.6 Ga Gawler Range Volcanics, South Australia. Journal of Volcanology and Geothermal Research 172, 132–147.

BARTON, M.D., & JOHNSON, D.A., 2004. Footprints Of Fe Oxide(-Cu-Au) Systems. *Centre For Global Metallogeny.* SEG Special Publication **33**. 112-116.

BARTON, M.D., 2014. Iron Oxide(-Cu-Au-Ree-P-Ag-U-Co) Systems. *Treatise On Geochemistry 2nd Edition.* 515-541.

BASTRAKOV, E.N., SKIRROW, R.G. AND DAVIDSON, G.J., 2007. Fluid evolution and origins of iron oxide Cu-Au prospects in the Olympic Dam District, Gawler craton, South Australia. Economic Geology 102, 1415-1440.

BELPERIO, A.P., FREEMAN, H., 2004. Common geological characteristics of Prominent Hill and Olympic Dam—implications for iron oxide copper-gold exploration models. Australasian Institute of Mining and Metallurgy Bulletin, Nov.-Dec. 2004, 67–75.

BELPERIO, A., FLINT, R. AND FREEMAN, H., 2007. Prominent Hill: A Hematite-Dominated, Iron Oxide Copper-Gold System. Economic Geology 102, 1499–1510.

BETTS, P.G., VALENTA, R.K., & FINLAY, J., 2003. Evolution Of The Mount Woods Inlier, Northern Gawler Craton: An Integrated Structural And Aeromagnetic Analysis. *Tectonophysics*, **366**, 83-111.

BETTS, P.G., GILES, D., SCHAEFER, B.F., MARK, G., 2007. 1600–1500 Ma hotspot track in eastern Australia: implications for Mesoproterozoic continental reconstructions. Terra Nova 19, 496–501.

BETTS, P.G., GILES, D., FODEN, J., SCHAEFER, B.F., MARK, G., PANKHURST, M.J., FORBES,C.J., WILLIAMS, H.A., CHALMERS, N.C., HILLS, Q.G., 2009. Mesoproterozoic plume-modified orogenesis in eastern Precambrian Australia. Tectonics 28, TC3006, doi:10.1029/2008TC002325.

CHALMERS, N.C., 2007a. Mount Woods Domain: Proterozoic Metasediments And Intrusives. *South Australia Department Of Primary Industries And Resources.* Report Book 2007/20.

CHALMERS, N.C., 2007b. The Mount Woods Domain: A Geological Review And Discussion On Mineralisation Potential. South Australia Department Of Primary Industries And Resources. Report Book 2007/7.

CONOR, C., RAYMOND, O., BAKER, T., TEALE, G., SAY, P. AND LOWE, G., 2010. Alteration and Mineralisation in the Moonta-Wallaroo Cu-Au Mining Field Region, Olympic Domain, South Australia. In: Porter, T.M. (Ed.), Hydrothermal Iron Oxide Copper-Gold and Related Deposits: A Global Perspective, vols. 3 and 4. PGC Publishing, Adelaide, p. 1-24.

CRAWFORD A.J., 2013. Petrographic Report: 4 samples from the Cairn Hill IOCG prospect, South Australia. *Report to IMX Resources Limited*. 1-21. (unpublished)

DALY, S.J., FANNING, C.M., FAIRCLOUGH, M.C., 1998. Tectonic evolution and exploration potential of the Gawler Craton, South Australia. AGSO Journal of Australian Geology and Geophysics 17 (3), 145-168.

DAVIDSON, G.J., PATERSON, H., MEFFRE, S., AND BERRY, R.F., 2007. Characteristics and origin of the Oak Dam East breccia-hosted, IOCG deposit: Olympic Dam region, Gawler Craton, SA. Economic Geology 102, 1471-1498.

DREXEL, J.F., PREISS, W.V., AND PARKER, A.J. 1993, The geology of South Australia: Volume 1, The Precambrian, South Australia: South Australia Geological Survey, *Bulletin 54*, p. 242.

EHRIG, K., MCPHIE, J., KAMANETSKY, V.S., 2013. Geology and mineralocigal zonation of the Olympic Dam iron oxide Cu-U-Au-Ag deposit, South Australia. In: Hedenquist, J.W., Harris, M., Camus, F. (Eds.), Geology and Genesis of Major Copper Deposits and Districts of the World, a Tribute to Richard Sillitoe. Society of Economic Geologists Special Publication 16, p. 237-268.

FANNING, C.M., FLINT, R.B., PARKER, A.J., LUDWIG, K.R., BLISSETT, A.H., 1988. Refined Proterozoic evolution of the Gawler Craton, South Australia, through U-Pb zircon geochronology. Precambrian Research 40/41, 363-386.

FANNING, C.M., 1993. Ion-microprobe U–Pb zircon dating of the Mount Woods Inlier, Preliminary Results (Unpublished). Research School of Earth Sciences, Australian National University, 8 pp.

FERRIS, G.M., SCHWARZ, M.P., & HEITHERSAY, P., 2002. The Geological Framework, Distribution And Control Of Fe-Oxide Cu-Au Mineralisation In The Gawler Craton, South Australia – Part 1. *Pgc Publishing - Hydrothermal Iron Oxide Copper-Gold & Related Deposits: A Global Perspective.* **2**. 33-47.

FLINT, R.B., & BENBOW, M.C., 1977. Geology Of The Mount Woods Inlier. *Department Of Mines Geological Survey. Report Book 77/134*

FORBES, C.J., GILES, D., HAND, M., BETTS, P.G., SUZUKI, K., CHALMERS, N., DUTCH, R., 2011.Using P–T paths to interpret the tectonothermal setting of prograde metamorphism: an example from the northeastern Gawler Craton, South Australia. Precambrian Research 185, 65–85.

FORBES, C.J. GILES, D. JOURDAN, F. SATO, K. OMORI, S. BUNCH, M 2012. Cooling And Exhumation History Of The Northeastern Gawler Craton, South Australia. Precambrian Research 200–203, 209-238.

FOSSEN H. 2010 Structural Geology. Cambridge University, New York, United States of America.

FREEMAN, H. AND TOMKINSON, M., 2011.Geological Setting of Iron Oxide Related Mineralisation in the Southern Mount Woods Domain, South Australia. In: Porter, T.M. (Ed.), Hydrothermal Iron Oxide Copper-Gold and Related Deposits: A Global Perspective, vols. 3 and 4. PGC Publishing, Adelaide, p. 171-190.

GROVES, D.I., BIERLEIN, F.P., MEINERT, L.D., HITZMAN, M.D., 2010. Iron Oxide Copper-Gold (Iocg) Deposits Though Earth History: Implications For Origin, Lithospheric Setting, And Distinction From Other Epigenetic Iron Oxide Deposits. *Economic Geology.* **105**. 641-654.

HAND, M., REID, A., & JAGODZONSKI, L., 2007. Tectonic Framework And Evolution Of The Gawler Craton, Southern Australia. *Economic Geology.* **102**. 1377-1395.

HAYNES, D.W., CROSS, K.C., BILLS, R.T., & REED, M.H., 1995. Olympic Dam Ore Genesis: A Fluid-Mixing Model. *Economic Geology.* **90**. 281-307.

HAYWARD, N. AND SKIRROW, R.G., 2010. Geodynamic setting and controls on iron oxide Cu-Au (±U) ore in the Gawler Craton, South Australia. In: Porter, T.M (Ed.), Hydrothermal Iron Oxide Copper-Gold & Related Deposits: A Global Perspective, Volume 3, PGC Publishing, Adelaide, p. 1-27.

HEMLEY, J.J., CYGAN, G.L., FEIN, J.B., ROBINSON, G.R., D'ANGELO, W.M. (1992) Hydrothermal ore-forming processes in the light of studies in rock-buffered systems. I. Iron-copper-zinc-lead sulfide solubility relations. Econ. Geol. 87:1 22

HITZMAN, M.W., ORESKES, N., & EINAUDI, M.T., 1992. Geological Characteristics And Tectonic Setting Of Proterozoic Iron Oxide (Cu-U-Au-Ree) Deposits. *Precambrian Research.* **58**. 241-287.

JAGODZINSKI, E.A., REID, A.J., CHALMERS, N., SWAIN, G., FREW, R.A., FOUDOULIS, C., 2007. Compilation Of Shrimp U–Pb Geochronological Data For The Gawler Craton, South Australia. *Department Of Primary Industries And Resources.* Report Book 2007/21.

MARK, G., OLIVER, N.H.S., WILLIAMS, P.J., VALENTA, R.K., AND CROOKES, R.A., 2000, The evolution of the Ernest Henry hydrothermal system, in Porter, T.M., ed., Hydrothermal iron oxide copper-gold and related deposits: A global perspective: Adelaide, Australian Mineral Foundation, p. 132–136.

MARK, G., OLIVER, N.H.S., AND WILLIAMS, P.J., 2006, Mineralogical and chemical evolution of the Ernest Henry Fe oxide-Cu-Au ore system, Cloncurry district, northwest Queensland, Australia, *Minerallium Deposita.* 40 pp. 769-801.

OLIVER, N.H.S., 2004, Modeling the role of sodic alteration in the genesis of iron-oxide-copper-gold deposits, Eastern Mt Isa Block, Australia. *Econ. Geol.* **99.** pp1145-1176

POLLARD, P.J., 2001, Sodic(-calcic) alteration associated with Fe-oxide-Cu-Audeposits: An origin via unmixing of magmatic-derived H2O-CO2-salt fluids: Mineralium Deposita, v. 36, p. 93–100.

POLLARD, P. J. 2006. An intrusion-related origin for Cu–Au mineralization in iron oxide–copper–gold (IOCG) provinces, *Mineralium Deposita* **41: 2**, 179-187. Porter, T.M., ed., 2000, Hydrothermal iron-oxide-copper-gold and related deposits: A global perspective: Australian Mineral Foundation, Adelaide, 349 pp.

PORTER, T.M., ED., 2000. Hydrothermal iron-oxide-copper-gold and related deposits: A global perspective, vol.1. PGC Publishing, Adelaide 367 pp.

PORTER, T.M., ED., 2002. Hydrothermal iron-oxide-copper-gold and related deposits: A global perspective. Advances in the Understanding of IOCG Deposits, vol. 2, PGC Publishing, Adelaide.

PORTER, T.M., 2010. The Carrapateena Iron Oxide Copper Gold Deposit, Gawler Craton, South Australia: a Review; in Porter, T.M., (ed.), Hydrothermal Iron Oxide Copper-Gold & Related Deposits: A Global Perspective, v. 3 - Advances in the Understanding of IOCG Deposits; PGC Publishing, Adelaide, pp. 1-10.

REED M.H. 1997. Hydrothermal alteration and its relationshipto ore fluid composition. In: Barnes H.L. (ed.), Geochemistry of Hydrothermal Ore Deposits, Wiley, New York, p. 303–365.

REEVE, J.S., CROSS, K.C., SMITH, R.N. AND ORESKES, N., 1990. Olympic Dam copper-uranium-gold-silver deposit. In Hughes, F.E. (Ed.), Geology of the Mineral Deposits of Australia and Papua New Guinea, Australasian Institute of Mining and Metallurgy, Monograph 14, p. 1009-1035.

REID,A.J., 2013. PACE Geochronology Project: PGC03-12: Geochronology of the Cairn Hill deposit, Mount Woods Inlier, South Australia. *Unpublished report.*, pp 1-18.

RICHARDS, J.P., AND MUMIN, A.H., 2013. Magmatic-hydrothermal processes within an evolving Earth: Iron-Oxide-copper-gold and porphyry Cu+Mo+Au deposits. *Geology.*,**41** pp 767-770.

ROTHERHAM, J.F., 1997. A metasomatic origin for the iron-oxide Au-Cu Starra orebodies, Eastern Fold Belt, Mount Isa Inlier, *Minerallium Deposita*, v. 32, pp. 205-218.

SEWARD T.M., BARNES H.L. 1997. Metal transportation by hydrothermal fluids. In: Barnes H.L. (ed.), *Geochemistry of Hydrothermal Ore Deposits*, 3rd ed, New York, Wiley, p. 435–486.Sillitoe, R.M., 2003. Iron oxide-copper gold deposits: An Andean view. Mineralium Deposita 38, 787-812.

SKIRROW, R.G., RAYMOND, O.L., BASTRAKOV, E., DAVIDSON, G. AND HEITHERSAY, P., 2002. The geological framework distribution and controls of Fe oxide Cu-Au mineralisation in the Gawler craton, SA. Part II. Alteration and mineralisation, in Porter, T.M., ed., Hydrothermal IOCG and related deposits: A global perspective: Adelaide, Australian Mineral Foundation, v. 2, p. 33-47.

SKIRROW, R.G., BASTRAKOV, E.N., BAROVICH, K., FRASER, G.L., CREASER, R., FANNING, M.C., RAYMOND, O.L. AND DAVIDSON, G.J., 2007.Timing of iron oxide Cu-Au-(U) hydrothermal activity and Nd isotope constraints on metal sources in the Gawler craton, South Australia. Economic Geology 102, 1441–1470.

STEWART, K., FODEN, J., 2001. Mesoproterozoic granites of South Australia, Department of Geology and Geophysics, University of Adelaide, unpub. report.

SWAIN, G., BAROVICH, K., HAND, M., FERRIS, G., SCHWARZ, M., 2008. Petrogenesis of the St Peter Suite, southern Australia: arc magmatism and Proterozoic crustal growth of the South Australian Craton. Precambrian Research 166, 283–296.

VANKO, D.A, & BISHOP, F.C,. 1982. Occurrence and origin of Marialitic Scapolite in the Humboldt Lopolith, N.W. Nevada. *Contrib. Mineral. Petrol,* **81**, pp. 277-289

VASSALLO, J, & WILSON, J,. 2001. Structural repetition of the Hutchison Group metasediments, Eyre Peninsula, South Australia. *Australian Journal of Earth Sciences,* **48**, 331

WILLIAMS, P.J., 1994, Iron mobility during synmetamorphic alteration in the Selwyn Range area, NW Queensland: Implications for the origin of iron-stone-hosted Au-Cu deposits: *Minerallium Deposita*.V.29, 250-260

WILLIAMS, P.J., BARTON, M.D., JOHNSON, D.A., FONTBOTÉ, L., DE HALLER, A., MARK, G., OLIVER, N.H.S. AND MARSCHIK, R., 2005, Iron oxide copper-gold deposits: Geology, Space-time distribution, and possible modes of origin. Economic Geology 100th Anniversary Volume, 371–405.

WILLIAMS, P.J., 2010a. Classifying IOCG Deposits. In: Corriveau, L. and Mumin, A.H., (eds.), Exploring for Iron Oxide Copper-gold Deposits: Canada and Global Analogues, Geological Association of Canada, Short Course Notes, vol. 20, pp. 13-21.

WILLIAMS, P.J., 2010b. "Magnetite-group" IOCGs with special reference to Cloncurry (NW Queensland) and Northern Sweden: Settings, alteration, deposit characteristics, fluid sources, and their relationship to apatite-rich iron ores. In: Corriveau, L. and Mumin, A.H., (eds.), Exploring for Iron Oxide Copper-gold Deposits: Canada and Global Analogues, Geological Association of Canada, Short Course Notes, vol. 20, pp. 23-38

APPENDIX A: DETAILED METHODOLOGY

Sampling

GEOLOGICAL MAPPING

Geological mapping, with an emphasis on primary structural and lithological controls on mineralisation, was undertaken on the two Cairn Hill operating open-pits. Pit 1 was nearing end of production and therefore was the primary focus of the mapping program due to accessibility; excavation of Pit 2 had only recently begun at time of field work. Mapping sheets for Pit's 1 and 2 were prepared by surveyors using a 1:1000 scale of the two open pits with a feint outline of the current open pit shape. Mapping of both pits followed the same method, systematic metre-by-metre face mapping starting at 0RL (surface) following the decline routes to the base of both pits. Reference points were strategically set-up across several benches in Pit 1 by the surveying team. Key features/relationships mapped were: Lithological changes (i.e. mineralogy and relative percentages); structures (fractures, joint sets, major and minor shear and/or brittle faults, vein systems, kinematic indicators); mineralisation and alteration presence and intensity (minerals (if determined), colour changes, habit, ore textures, breccias, intensity based on relative percentage of host lithology present).

SAMPLE COLLECTION & PREPARATION

Approximately sixty samples were collected from exposed faces immediately accessible via the decline ramp in both Pits 1 and 2 using a geo-pick. The aim was to collect a samplesuite representative of the Cairn Hill deposit, including primary to secondary mineralised ore zones, host lithologies and subsequent alteration haloes across the deposit. Fresh host rock samples were also collected. Sample sizes were variable depending on individual rock properties across lithologies and alteration assemblages. Generally, samples were 10cm x10cm x 5cm with weight ranging from 1kg (granitic to weakly altered lithologies) to approximately 5kg (massive magnetite-rich ore zones).

Forty selected samples were prepared for thin sections or polished block based on their degree of alteration and mineralisation. The final selection are most representative of the deposit, the remainder of samples were discarded primarily due to similarity. Samples were cut using the diamond blade rock saw at Adelaide University into 3 x 1inch blocks for final preparation as polished blocks and polished thin sections at Adelaide Petrographic Laboratories.

DRILL-CORE LOGGING

Approximately 1000m of drill-core was logged across two drill-holes at the Glenside Core Library under permission from DMITRE geologists. The deep-copper drill-holes program commenced in 2012 under a joint venture with Oz Minerals and IMX Resources, in order to determine absolute depths of copper mineralisation. The two drill-holes begin at surface and go to depths in excess of 200 metres, intersecting both primary ore-lodes, along with a representative intersection of alteration assemblages present and unaltered host lihologies.
Selection criteria considered:

- Representative samples for different lithologies.
- Representative samples for different alteration styles
- Presence of iron oxides, particularly hematite and magnetite transformation
- Presence of sulphides, particularly Cu bearing sulphides.
- Presence of veining.

Analytical Methodology

PETROGRAPHIC ANALYSIS

The Nikon LV100 polarising petrographic microscope analysed all forty samples and represents the first stage of petrographic analysis. The Nikon LV100 microscope has the magnification capacity up to 50x and can function with both transmitted and reflected light modes. Software and camera packages were used to image minerals, mineral relationships and textures of interest.

Analysis of samples using transmitted light focussed on the size, distribution, zonation, textures and relationships of:

- Feldspars - microcline/plagioclase (albite)
- Alteration minerals - amphibole/biotite/quartz/chlorite/carbonate
- Accessory minerals - rutile/zircon/monazite
- Analysis of samples using reflected light focussed on the size, distribution, zonation,
- textures and relationships of:
- Iron-oxides - magnetite/hematite
- Sulphides - pyrite/chalcopyrite/pyhrrotite
- Accessory minerals - rutile/zircon/monazite

QUANTA 450 FEI SCANNING ELECTRON MICROSCOPE (SEM)

Samples were first carbon coated by Adelaide Microscopy staff for use on the Quanta 450 SEM. The Instrument includes EDAX TEAM Energy Dispersive X-ray Spectroscopy (EDS) with silicon drift detector (SDD) detector and back-scatter electron (BSE) detector. The Quanta SEM was operated in back-scatter mode (BSE) for interpretation and imaging for all samples, using an accelerated voltage of 20k at a spot size of 4 microns. Software and camera packages were used to image minerals, mineral relationships and textures of interest.

The BSE imaging allowed observations on minerals of interest, including their speciation and the micro-scale association between gangue, alteration and ore minerals. Their fine textures, mineral intergrowths, compositional zoning and inclusions were also observed and captured. Qualitative mineral analyses were performed using EDAX software providing additional information regarding mineral compositions and chemical exchange.

References

COOK, N.J., CIOBANU, C.L., GILES, D. & WADE, B., 2013. Correlating textures and trace elements in ore minerals. In: Mineral deposit research for a high-tech world. 12th Biennial SGA Meeting, 12-15 August 2013, Uppsala, Sweden. 288-291.

FLANAGAN F.J., 1976, Descriptions and Analysis of Eight New USGS Rock Standards: U.S. Geological Survey Professional Paper **840**, 192.

APPENDIX B: RESULTANT CORE LOGGING REPORTS

CHDCu001 - Core Logging Report

HOLE	Core Depth (m)		Lithology	Description	Best Cu grade
CHDCu02	Start	End			
CHDCu02	0	39	COVER SEQUENCE	Mesozoic to Permian sediments. Cadna-owie sands and silts predominant lithology represented at Cairn Hill	
CHDCu02	39	132.5	Balta alkali-Granite (foliated)	Qtz-K-feldspar-biotite +/- plagioclase-magnetite-hornblende. Bt defines foliation. Minor disseminated magnetite. “Mottled” black hornblende evident as an alteration product of predominately feldspars +/- mafic minerals. Wide qtz veins (~10cm) evident following foliation trend. Black Chl alteration of bt-rich foliation/ mineralogical bands. Mnr soft red hem-yellow ser+/-clays veins. @44m hem-ser breccia infill.	

CHDCu02	132.5	144.5	QFBM gneiss	Magnetite-black chlorite-green amphibole-biotite strongly foliated altered rock. Diffuse boundaries with GG. >30% magnetite content.	
CHDCu02	144.5	149	altered gabbro dyke	Sharp contact with GG; different to other mafic-gneiss units that are usually diffuse and appear as massive mag. Predominantly mag-rich +/- plagioclase and mnr qtz. Looks Doleritic/Basaltic. Mnr qtz veins evident, and have been folded. Mnr sulphide (py) mineralisation evident associated with qtz veining.	
CHDCu02	149	172	Balta alkali-Granite (foliated)	Qtz-K-feldspar-biotite +/- plagioclase-magnetite-hornblende. Bt defines foliation. Minor disseminated magnetite. Wide qtz veins (~10cm) evident following foliation trend. Black Chl alteration of bt-rich foliation/ mineralogical bands. Mnr soft red hem-yellow ser+/-clays veins.	
CHDCu02	172	189	QFBM gneiss	High magnetite content (<10%). High strain and increased quartz (folded) and biotite veining/compositional layering. Approaching ductile shear zone?	
CHDCu02	189	207	MB schist - Orebody	100% Bt-Mag +/- micas (muscovite) Hydrous ductile? shear zone. Qtz veins are evident with ser/chl alteration evident on the margins of qtz associated with py+/- cpy mineralisation. Magnetite-rich zone.	
CHDCu02	230	255.5	QFBM gneiss	High magnetite content (<10%). High strain and increased quartz (folded) and biotite veining/compositional layering.	
CHDCu02	255.5	339	Mylonite	Mylonitized zone of granite gneiss. Mafic layers characterised by predominantly bt +/- magnetite. Mnr “xenoliths” or leucosomic zones of qtz-k-feldspar. Variable zones of mineralisation associated with chlorite-quartz-amphibole alteration in magnetite-rich zones. @361m (creamy coloured) albitite cuts foliation: ~1m interval	
CHDCu02	339	382.1	QFBM gneiss	Relatively consistent zone. Predominantly mag-bt- rich zones defining foliation with pockets of qtz-k-feldspar evident - Migmatitic. @ 400-410m interval contains enriched amphibole-chlorite+/- epidote alteration within ‘mafic’ zones.	
CHDCu02	382.1	391.5	Calcic-skarn	Di-mag-hornblende skarn cuts foliation. However, may represent metamoprhic re-crystallisation. Interbedded? Zones of hornblendite (amphibolites)	**Best Assay results. 0.11% Cu between**

					382m - 382.89m
CHDCu02	391.5	418	QFBM gneiss	Relatively consistent zone. Predominantly mag-bt- rich zones defining foliation with pockets of qtz-k-feldspar evident - Migmatitic. @ 400-410m interval contains enriched amphibole-chlorite+/- epidote alteration within 'mafic' zones.	
CHDCu02	418	427	Mylonite (M)	Mylonitization of QFBM-gneiss is evident indicated by high strain, grain-reduced granitic minerals, with syn pegmatitic-granite dykes intruding folding the mylonite. Therefore indicates a high-temperature regime.	
CHDCu02	427	434	QFBM gneiss	Migmatitic (granite-gneiss) predominantly represented by strong bt-mag+/-green amphiboles-black chlorite layering defining foliation. Qtz-K-feldspar leucosomic melts evident.	
CHDCu02	434	441.5	Calcic-skarn	Di-mag-hornblende skarn cuts foliation. However, may represent metamoprhic re-crystallisation. Interbedded? Zones of hornblendite (amphibolites)	
CHDCu02	441	460	altered gabbro dyke	Sharp contact with GG; different to other mafic-gneiss units that are usually diffuse and appear as massive mag. Predominantly mag-rich +/- plagioclase and mnr qtz. Looks Doleritic/Basaltic. Mnr qtz veins evident, and have been folded. Mnr sulphide (py) mineralisation evident associated with qtz veining.	
CHDCu02	460	470	QFBM gneiss	Migmatitic - as describe above. Later qtz veins cross-cut foliation. Green-amphiboles associated with mag-bt following foliation trend.	
CHDCu02	470	474	Pegmatite	coarse-grained K-feldspar-quartz and moderate tourmaline. Sheared.	
CHDCu02	474	550.1	QFBM gneiss	Qtz-K-feldspar-biotite +/- plagioclase-magnetite-hornblende. Bt defines foliation. Minor disseminated magnetite. Wide qtz veins (~10cm) evident following foliation trend. Black Chl alteration of bt-rich foliation/ mineralogical bands.	
EOH	EOH	EOH	EOH	EOH	

CHDCu002 - Core Logging Report

HOLE	Core Depth (m)	Lithology	Description	Best Cu grade

CHDCu02	Start	End			
CHDCu02	113.2	276.5	COVER SEQUENCE	Mesozoic to Permian sediments. Cadna-owie sands and silts predominant lithology represented at Cairn Hill	
CHDCu02	276.5	329	CORE LOST	CORE LOST	
CHDCu02	329	329.5	Conglomerate	Unconformable contact with Hiltaba-aged Granite-gneiss.	
CHDCu02	329.5	330.5	Balta alkali-Granite (foliated)	Qtz-K-feldspar-biotite +/- plagioclase-magnetite-hornblende. Bt defines foliation. Minor disseminated magnetite. “Mottled” black hornblende evident as an alteration product of predominately feldspars +/- mafic minerals. Wide qtz veins (~10cm) evident following foliation trend. Black Chl alteration of bt-rich foliation/ mineralogical bands. Mnr soft red hem-yellow ser+/-clays veins	
CHDCu02	330.5	332.5	QFBM gneiss	Magnetite-black chlorite-green amphibole-biotite strongly foliated altered rock. Diffuse boundaries with GG. >30% magnetite content.	
CHDCu02	332.5	330	QFBM gneiss	High magnetite content (<10%). High strain and increased quartz (folded) and biotite veining/compositional layering. Approaching ductile shear zone?	
CHDCu02	330	336.5	QFBM gneiss	Sharp contact with GG; different to other mafic-gneiss units that are usually diffuse and appear as massive mag. Predominantly mag-rich +/- plagioclase and mnr qtz. Looks Doleritic/Basaltic. Mnr qtz veins evident, and have been folded. Mnr sulphide (py) mineralisation evident associated with qtz veining.	
CHDCu02	336.5	337	QFBM gneiss	Thin interval of GG as interpreted in above intervals.	
CHDCu02	337	338.5	Bt-schist (BS)	100% Bt +/- micas (muscovite) OR schistose (metamorphosed) sulphides (i.e. py). Hydrous ductile? shear zone. Qtz veins are evident with ser/chl alteration evident on the margins of qtz associated with py+/- cpy mineralisation	
CHDCu02	338.5	350	QFBM gneiss	Diffuse boundary (i.e. slow decrease in mafic (bt +/- mag) mineralogical layering. Highly fractured. Perhaps it is a brittle-ductile? shear zone? Disseminated sulphides (py +/- cpy) evident along qtz-grain margins, within chloritized clasts, magnetite and/or associated with black hornblende (amphibole). High strain evidenced by crystalline qtz as elongated qtz-	

				ribbons.	
CHDCu02	350	351	Bt-schist	+/- clay alteration evident. Potentially fault gouge - as highly rubble.	
CHDCu02	351	359	QFBM gneiss	As above.	
CHDCu02	359	361	MB schist	As above.	
CHDCu02	361	379	Mylonite (M)	Mylonitization of granite-gneiss is evident indicated by high strain, grain-reduced granitic minerals, with syn pegmatitic-granite dykes intruding folding the mylonite. Therefore indicates a high-temperature regime.	
CHDCu02	379	381	QFBM gneiss	Migmatitic (granite-gneiss) predominantly represented by strong bt-mag+/-green amphiboles-black chlorite layering defining foliation. Qtz-K-feldspar leucosomic melts evident.	
CHDCu02	381	383	QFBM gneiss	As above (previous interval)	
CHDCu02	383	390.5	QFBM gneiss	Migmatitic - as describe above. Later qtz veins cross-cut foliation. Green-amphiboles associated with mag-bt following foliation trend.	
CHDCu02	390.5	395	Balta alkali-Granite (foliated)	Relatively “fresh” granite dyke. Weakly foliated, defined by bt. Predominantly K-feldspar - rich, with qtz-plag. K-spar may be a mixture of remnant albitization (i.e. red-rock-alteration). No Mineralisation (i.e. sulphides).	
CHDCu02	395	400	Mylonite	Mylonitized zone of granite gneiss. Mafic layers characterised by predominantly bt +/- magnetite. Mnr “xenoliths” or leucosomic zones of qtz-k-feldspar.	
CHDCu02	400	431	QFBM gneiss	Relatively consistent zone. Predominantly mag-bt- rich zones defining foliation with pockets of qtz-k-feldspar evident - Migmatitic. @ 400-410m interval contains enriched amphibole-chlorite+/- epidote alteration within ‘mafic’ zones.	**Best Assay results. 0.79% Cu between <u>402m - 403m</u>**
CHDCu02	431	436	Granite-gneiss	Qtz-K-feldspar-biotite +/- plagioclase-magnetite-hornblende. Bt defines foliation. Sulphide (Py) mineralisation evident on Qtz grain-boundaries as well as following foliation trends associated with mag. @434.6m Late stage carbonate veining evident, cross-cutting all alteration and metamorphic fabric.	

CHDCu02	436	449.8	QFBM gneiss	As above.	
EOH	EOH	EOH	EOH	EOH	

CHDCu003 - Core Logging Report

HOLE	Core Depth (m)		Lithology	Description	Best Cu grade
CHDCu03	Start	End			
CHDCu03	113.2	276.5	COVER SEQUENCE	Mesozoic to Permian sediments. Cadna-owie sands and silts predominant lithology represented at Cairn Hill	
CHDCu03	276.5	329	CORE LOST	CORE LOST	
CHDCu03	329	329.5	Conglomerate	Unconformable contact with Hiltaba-aged Granite-gneiss.	
CHDCu03	329.5	330.5	Balta alkali-Granite (foliated)	Qtz-K-feldspar-biotite +/- plagioclase-magnetite-hornblende. Bt defines foliation. Minor disseminated magnetite. “Mottled” black hornblende evident as an alteration product of predominately feldspars +/- mafic minerals. Wide qtz veins (~10cm) evident following foliation trend. Black Chl alteration of bt-rich foliation/ mineralogical bands. Mnr soft red hem-yellow ser+/-clays veins	
CHDCu03	330.5	332.5	QFBM gneiss	Magnetite-black chlorite-green amphibole-biotite strongly foliated altered rock. Diffuse boundaries with GG. >30% magnetite content.	
CHDCu03	332.5	330	Balta alkali-Granite (foliated)	High magnetite content (<10%). High strain and increased quartz (folded) and biotite veining/compositional layering. Approaching ductile shear zone?	
CHDCu03	330	336.5	altered gabbro dyke	Sharp contact with GG; different to other mafic-gneiss units that are usually diffuse and appear as massive mag. Predominantly mag-rich +/- plagioclase and mnr qtz. Looks Doleritic/Basaltic. Mnr qtz veins evident, and have been folded. Mnr sulphide (py) mineralisation evident associated with qtz veining.	
CHDCu03	336.5	337	Balta alkali-Granite (foliated)	Thin interval of GG as interpreted in above intervals.	

CHDCu03	337	338.5	MB schist	100% Bt +/- micas (muscovite) OR schistose (metamorphosed) sulphides (i.e. py). Hydrous ductile? shear zone. Qtz veins are evident with ser/chl alteration evident on the margins of qtz associated with py+/- cpy mineralisation	
CHDCu03	338.5	350	Balta alkali-Granite (foliated)	Diffuse boundary (i.e. slow decrease in mafic (bt +/- mag) mineralogical layering. Highly fractured. Perhaps it is a brittle-ductile? shear zone? Disseminated sulphides (py +/- cpy) evident along qtz-grain margins, within chloritized clasts, magnetite and/or associated with black hornblende (amphibole). High strain evidenced by crystalline qtz as elongated qtz-ribbons.	
CHDCu03	350	351	MB schist	+/- clay alteration evident. Potentially fault gouge - as highly rubble.	
CHDCu03	351	359	Balta alkali-Granite (foliated)	As above.	
CHDCu03	359	361	MB schist	As above.	
CHDCu03	361	379	Mylonite (M)	Mylonitization of granite-gneiss is evident indicated by high strain, grain-reduced granitic minerals, with syn pegmatitic-granite dykes intruding folding the mylonite. Therefore indicates a high-temperature regime.	
CHDCu03	379	381	QFBM gneiss	Migmatitic (granite-gneiss) predominantly represented by strong bt-mag+/-green amphiboles-black chlorite layering defining foliation. Qtz-K-feldspar leucosomic melts evident.	
CHDCu03	381	383	Balta alkali-Granite (foliated)	As above (previous interval)	
CHDCu03	383	390.5	QFBM gneiss	Migmatitic - as describe above. Later qtz veins cross-cut foliation. Green-amphiboles associated with mag-bt following foliation trend.	
CHDCu03	390.5	395	Granite	Relatively “fresh” granite dyke. Weakly foliated, defined by bt. Predominantly K-feldspar - rich, with qtz-plag. K-spar may be a mixture of remnant albitization (i.e. red-rock-alteration). No Mineralisation (i.e. sulphides).	

CHDCu03	395	400	Mylonite	Mylonitized host rock. Mafic layers characterised by predominantly bt +/- magnetite. Mnr “xenoliths” or leucosomic zones of qtz-k-feldspar.	
CHDCu03	400	431	QFBM gneiss	Relatively consistent zone. Predominantly mag-bt- rich zones defining foliation with pockets of qtz-k-feldspar evident - Migmatitic. @ 400-410m interval contains enriched amphibole-chlorite+/- epidote alteration within ‘mafic’ zones.	
CHDCu03	431	436	Balta alkali-Granite (foliated)	Qtz-K-feldspar-biotite +/- plagioclase-magnetite-hornblende. Bt defines foliation. Sulphide (Py-Ccp) mineralisation evident on Qtz grain-boundaries as well as following foliation trends associated with mag. @434.6m Late stage carbonate veining evident, cross-cutting all alteration and metamorphic fabric.	**Best Assay results. 0.9% Cu between <u>434.0-434.6m</u>**
CHDCu03	436	449.8	QFBM gneiss	As above.	